On the evaluation of the Eshelby tensor for polyhedral inclusions of arbitrary shape

S. Trotta[a], G. Zuccaro[a,b], S. Sessa[a], F. Marmo[a], L. Rosati[a]

[a] *Department of Structures for Engineering and Architecture, University of Naples Federico II, Via Claudio, 21, 80124 Napoli, Italy*
[b] *Corresponding author*

Abstract

We derive the analytical expression of the Eshelby tensor field for inclusions of arbitrary polyhedral shape. The formula contributed in the paper is directly expressed as function of the coordinates defining the vertices of the polyhedron thus avoiding the use of complex variables and anomalies exploited in previous contributions on the subject. It has been obtained by evaluating analytically the integrals appearing in the very definition of the Eshelby tensor by means of two consecutive applications of the Gauss theorem.

The first one allows one to express the original volume integrals as a sum of 2D integrals extended to the faces of the polyhedron, while the second application transforms each 2D integral into the line integrals extended so the edges of each face.

The effectiveness of the proposed formulation is numerically assessed by comparing the results provided by its implementation in a Matlab code with results available in the literature.

Keywords: Eshelby tensor, Polyhedral inclusion, Micromechanics, Analytical solution.

1. Introduction

The presence of inclusions in engineering materials affects their elastic fields, at the local and global scale, thus greatly influencing their mechanical and physical properties.

In particular composite materials take advantage of inclusions as reinforcements in the matrix in order to achieve superior properties that, otherwise, could not be obtained by individual constituent materials [1].

In other cases inclusions are unintentionally but inevitably formed during the material manufacturing process, such as oxides, carbides and voids in steel, and act as sources of stress concentration that affect performance and endurance of the material. Hence the study of inclusions plays an important role in the development of advanced materials for aerospace, marine, automotive and several additional applications.

Inclusions are usually categorized [2, 3] into homogeneous, inhomogeneous and inhomogeneities. Homogeneous inclusions have the same elastic moduli as the surrounding host or matrix material but contain the so called eigenstrain, i.e. a non elastic strain such as thermal expansion [4, 5] , phase transformation [6], visco-plastic strain [7] misfit strain [8] of quantum dot structures [9].

An inhomogeneous inclusion not only contains an eigenstrain but has also elastic moduli different from those of the matrix. Differently from the previous case an inhomogeneity does not contain an eigensrain.

The study of inclusions was pioneered by Eshelby in a celebrated paper [10] in which he considered an ellipsoidal inhomogeneous inclusion in an infinite matrix by simulating it as a homogeneous inclusion with an initial eigenstrain plus a properly selected equivalent eigenstrain. The ellipsoidal inclusion had uniform eigenstrain and stress if the initial eigenstrain within it was uniform.

The basic tool of this approach, denominated Equivalent Inclusion Method (EIM), was the Eshelby tensor, i.e. a fourth-order tensor relating the total strain to the eigenstrain, expressed as second derivative of the Green function of the elastic medium.

The EIM has allowed the effects of inclusions to be studied extensively and has been summarized in classical references, such as the review papers by Mura and co-workers [11, 12, 13, 14] and in several books [15, 16, 17, 18, 19]. Comprehensive reviews addressing applications of the EIM in micromechanics and homogeneization can be found in [20, 21, 22, 23].

Of particular relevance is the combination of the Eshelby theory with the Mori-Tanaka approach [24] for an accurate prediction of the effective thermomechanical properties of composites. Actually, just to quote some of the most recent contributions on the subject, the Eshelby-Mori-Tanaka mean-field theory has been applied in several contexts ranging from damage mechanics of cement concrete [25], to periodic composites [26], to micromechanical models of carbon nanotube composites [27, 28, 29, 30] to multi-coating micromechanics accounting for interphase behaviour [31, 32], to the analysis of thermal stresses developed in ceramic matrix composites [33] or hybrid nanocomposites [34], to studies concerning the influence of size effects in the evaluation of macroscopic properties of multifunctional nanocomposites [35, 36].

Although Eshelby tensor theory has been conceived for elliptical (ellipsoidal) inclusions, mainly to simplify the analytical treatment, non-elliptical (non-ellipsoidal) inclusions are of great practical importance for applications [37]. For instance polygonal or polyhedral SiC whiskers are used in metal and ceramic matrix composites, or eutectics in superconductor composites. Furthermore several modern semiconductor devices, such as lasers, infrared detectors and information storage de-

vices use composite materials in which objects having the size of several nanometers are buried in the surrounding matrix [9, 38].

Since the elastic deformation produced by inclusions are described by harmonic and bi-harmonic potentials [10], Rodin [39] adopted the Waldvogel's algorithm [40] for the Newtonian potential to formulate a two-dimensional plane strain problem for the polygonal section of an infinite cylinder.

The solution contributed by Rodin was cumbersome and the programming implementation of his algorithm required ad-hoc strategies such as coordinate rotation. In two subsequent papers Nozaki-Taya derived a rather involved expression of the Eshelby tensor for convex [41] and non convex [42] inclusions obtained as a function an of the rays connecting the observation point with the vertices of the polygon.

Further results on the Eshelby tensor of 2D inclusions of a arbitrary shape have been contributed in [43], by using techniques of analytical continuation and conformal mapping, or in [44, 45] exploiting special properties of tensors proved in [46].

In two recent papers [47, 48], limited to the case of 2D inclusions, effective formulas for the Eshelby tensor have been obtained by exploiting recent results for the Newtonian potential [49, 50], and subsequently applied to several problems ranging from geophysics [51, 52], to geomechanics [53, 54] and to heat transfer [55].

To the best of the author's knowledge papers providing analytical evaluation of the Eshelby tensor of 3D inclusions of arbitrary shape are scarce, the only remarkable exceptions being the contributions by Gao and Liu [56], although devoted to gradient elasticity, and Wang et al [57].

Hence, aim of this paper is to derive a particularly compact and effective expressions by suitably generalizing the approach presented in [47]. In particular we consider a first application of the Gauss theorem to express the volume integral extended to the polyhedral domain as sum of area integrals extended to the faces bounding the polyhedron.

A further application of the Gauss theorem transforms the face integrals into line integrals, extended to the edges of each face, that are analytically evaluated, thus allowing for closed-form expression of the Eshelby tensor.

Remarkably, differently from previous contributions, our formula is directly expressed as function of the position vectors defining the vertices of the polyhedron, i.e. the basic geometric elements used to assign the inclusion.

The numerical assessment of the novel formula for the Eshelby tensor has been carried out by means of a Matlab code. Several examples related to different shape inclusions [56] prove the effectiveness of the proposed approach.

2. The Eshelby tensor

Let us consider an infinite, elastic, homogeneous and isotropic space having an arbitrarily shaped inclusion Ω in which a uniform eigenstrain $\boldsymbol{\varepsilon}^*$ is assigned. Furthermore we introduce a Cartesian reference frame of origin O and axis x_1, x_2 and x_3 as shown in Fig. 1

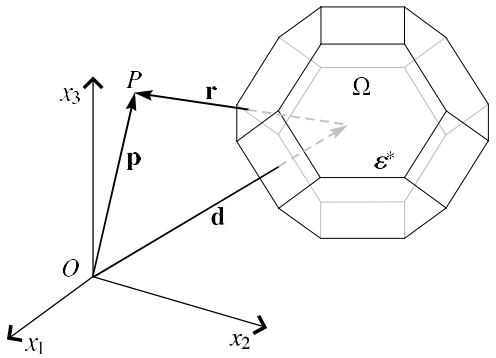

Figure 1: A polyhedral inclusion Ω

Adopting index notation, the displacement $\mathbf{u}$ generated by the inclusion at a point P of position $\mathbf{p} = (p_1, p_2, p_3)$ is expressed as [3]

$$u_i(\mathbf{p}) = -\left[\int_\Omega \frac{\partial G_{ik}}{\partial p_l}(\mathbf{p}-\mathbf{d})\, d\mathbf{d}\right] C_{klmn}\varepsilon^*_{mn} = \\ = -\left[\int_\Omega G_{ik,l}(\mathbf{r})\, d\mathbf{r}\right] C_{klmn}\varepsilon^*_{mn} \tag{1}$$

where $\mathbf{d} = (d_1, d_2, d_3)$ is the position of a generic point inside the inclusion and the vector $\mathbf{r} = \mathbf{p} - \mathbf{d}$ has been introduced to simplify the notation. The comma in the last formula denotes differentiation with respect to r_l.

The tensor $\mathbf{G}$ is the Green's function in the case of three-dimensional elasticity and its expression is [3]

$$\mathbf{G}(\mathbf{r}) = \frac{1}{16\pi\mu(1-\nu)}\left[\frac{\mathbf{r}\otimes\mathbf{r}}{(\mathbf{r}\cdot\mathbf{r})^{3/2}} + (3-4\nu)\frac{\mathbf{I}}{(\mathbf{r}\cdot\mathbf{r})^{1/2}}\right] \tag{2}$$

where μ is the shear modulus, ν is the Poisson's ratio and $\mathbf{I}$ is the three-dimensional identity tensor. In index notation the previous relation becomes

$$G_{ik} = U\left[\frac{r_i\, r_k}{(\mathbf{r}\cdot\mathbf{r})^{3/2}} + V\frac{\delta_{ik}}{(\mathbf{r}\cdot\mathbf{r})^{1/2}}\right]_{ik} \tag{3}$$

where $U = 1/[16\pi\mu(1-\nu)]$ and $V = 3-4\nu$.

The elasticity tensor $\mathbb{C}$ used in formula (1) is expressed in index notation as

$$C_{klmn} = \lambda\delta_{kl}\delta_{mn} + \mu(\delta_{km}\delta_{ln} + \delta_{kn}\delta_{lm}) \tag{4}$$

where λ is the first Lamé constant.

The infinitesimal strain tensor $\boldsymbol{\varepsilon}$ at P can be evaluated as a function of the displacement $\mathbf{u}$ by differentiating formula (1). Accordingly one has

$$\varepsilon_{ij} = \frac{1}{2}\left(u_{i,j} + u_{j,i}\right) = \\ = -\frac{1}{2}\left[\int_\Omega G_{ik,lj}(\mathbf{r})dV + \int_\Omega G_{jk,li}(\mathbf{r})dV\right] C_{klmn}\varepsilon^*_{mn} = \\ = S_{ijmn}(P)\varepsilon^*_{mn} \tag{5}$$

where the fourth-order tensor

$$S_{ijmn}(P) = -\frac{1}{2}\left[\int_{\Omega} G_{ik,lj}(\mathbf{r})dV + \int_{\Omega} G_{jk,li}(\mathbf{r})dV\right]C_{klmn} \quad (6)$$

is the Eshelby tensor for three-dimensional elasticity.

We apply the Gauss theorem to transform the volume integrals, extended to the region Ω occupied by the inclusion, into area integrals, extended to the boundary $\partial\Omega$ of the inclusion. Hence, the Eshelby tensor (6) is rewritten as

$$S_{ijmn}(P) = -\frac{1}{2}\left\{\int_{\partial\Omega} G_{ik,j}(\mathbf{r})n_l(\mathbf{r})dA + \int_{\partial\Omega} G_{jk,i}(\mathbf{r})n_l(\mathbf{r})dA\right\}C_{klmn} \quad (7)$$

where $\mathbf{n}$ is the outward unit vector orthogonal to $\partial\Omega$.

The gradient of the Green function appearing as argument of the two integrals in the previous equation can be obtained by differentiating formula (3). Accordingly, one has

$$G_{ik,j} = U\left\{-3\frac{r_i r_k r_j}{(\mathbf{r}\cdot\mathbf{r})^{\frac{5}{2}}} + \delta_{ij}\frac{r_k}{(\mathbf{r}\cdot\mathbf{r})^{\frac{3}{2}}} + \frac{r_i}{(\mathbf{r}\cdot\mathbf{r})^{\frac{3}{2}}}\delta_{kj} - V\frac{r_j}{(\mathbf{r}\cdot\mathbf{r})^{\frac{3}{2}}}\delta_{ik}\right\} \quad (8)$$

Substituting formula (8) into (7) we obtain the following expression for the first integral appearing in the expression of the Eshelby's tensor

$$\int_{\partial\Omega} G_{ik,j}n_l dA = U\left\{-3\Upsilon_{ikjl} + \delta_{ij}\omega_{kl} + \omega_{il}\delta_{kj} - V\omega_{jl}\delta_{ik}\right\} \quad (9)$$

where

$$\omega_{il} = \int_{\partial\Omega}\frac{r_i\, n_l}{(\mathbf{r}\cdot\mathbf{r})^{\frac{3}{2}}}dA\,, \quad \Upsilon_{ijkl} = \int_{\partial\Omega}\frac{r_i r_k r_j\, n_l}{(\mathbf{r}\cdot\mathbf{r})^{\frac{5}{2}}}dA \quad (10)$$

The second integral in (7) has an expression similar to (9) by exchanging the indexes i and j and observing that $\Upsilon_{ijkl} = \Upsilon_{jikl}$

The formulas for evaluating the integrals in (10) are obtained in section 3 while here they are used to express the Eshelby tensor as

$$S_{ijmn}(P) = -\frac{U}{2}\left(2\delta_{ij}\omega_{kl} + \omega_{il}\delta_{kj} + \omega_{jl}\delta_{ki} - 6\,\Upsilon_{ijkl} - 2V\delta_{ik}\omega_{jl} - 2V\delta_{jk}\omega_{il}\right)C_{klmn} \quad (11)$$

where the identities $\delta_{ij} = \delta_{ij}$ and $\Upsilon_{ijkl} = \Upsilon_{jikl}$ have been used. Finally, substituting formula (4) into the previous expression one has

$$S_{ijmn}(P) = -\frac{U}{2}\Big[2\lambda\omega_{ll}\delta_{ij}\delta_{mn} + 2\mu(\omega_{nm} + \omega_{mn})\delta_{ij} + (\lambda - 2V\lambda)(\omega_{ij} + \omega_{ji})\delta_{mn} + (\mu - 2V\mu)(\omega_{in}\delta_{jm} + \omega_{jn}\delta_{im} + \omega_{im}\delta_{jn} + \omega_{jm}\delta_{in}) - 6\lambda\Upsilon_{ijll}\delta_{mn} - 6\mu(\Upsilon_{ijmn} + \Upsilon_{ijnm})\Big] \quad (12)$$

which fulfils minor symmetries.

Adopting a Voigt notation $[\boldsymbol{\varepsilon}]_V$ for simmetric second-order tensor $[\boldsymbol{\varepsilon}]$

$$[\boldsymbol{\varepsilon}] = \begin{bmatrix} \varepsilon_{11} & \varepsilon_{12} & \varepsilon_{13} \\ \varepsilon_{21} & \varepsilon_{22} & \varepsilon_{23} \\ \varepsilon_{31} & \varepsilon_{32} & \varepsilon_{33} \end{bmatrix} \quad \Leftrightarrow \quad [\boldsymbol{\varepsilon}]_V = \begin{bmatrix} \varepsilon_{11} \\ \varepsilon_{22} \\ \varepsilon_{33} \\ 2\varepsilon_{12} \\ 2\varepsilon_{13} \\ 2\varepsilon_{23} \end{bmatrix} \quad (13)$$

the Eshelby tensor can be expressed as

$$[S]_V = \begin{bmatrix} S_{1111} & S_{1122} & S_{1133} & 0 & 0 & 0 \\ S_{2211} & S_{2222} & S_{2233} & 0 & 0 & 0 \\ S_{3311} & S_{3322} & S_{3333} & 0 & 0 & 0 \\ 0 & 0 & 0 & 2S_{1212} & 0 & 0 \\ 0 & 0 & 0 & 0 & 2S_{1313} & 0 \\ 0 & 0 & 0 & 0 & 0 & 2S_{2323} \end{bmatrix} \quad (14)$$

3. Analytical expression of the boundary integrals in terms of face integrals

For a polyhedral inclusion, whose boundary $\partial\Omega$ is made of N_F faces, the integrals (10) can be further specialized as follows

$$\omega_{il} = \sum_{f=1}^{N_F}\left(\boldsymbol{\omega}^f \otimes \mathbf{n}_f\right)_{il}, \quad \Upsilon_{ijkl} = \sum_{f=1}^{N_F}\left(\boldsymbol{\Upsilon}^f \otimes \mathbf{n}_f\right) = \Upsilon^f_{ijk}(\mathbf{n}_f)_l \quad (15)$$

where

$$\boldsymbol{\omega}^f = \int_{F_f}\frac{\mathbf{r}_f}{(\mathbf{r}_f\cdot\mathbf{r}_f)^{\frac{3}{2}}}dA_f\,, \quad \boldsymbol{\Upsilon}^f = \int_{F_f}\frac{\mathbf{r}_f\otimes\mathbf{r}_f\otimes\mathbf{r}_f}{(\mathbf{r}_f\cdot\mathbf{r}_f)^{\frac{5}{2}}}dA_f \quad (16)$$

and $\mathbf{n}_f$ is the unit vector normal to the f-th face pointing outwards Ω.

To express the previous 2D integrals in terms of line integrals, we need a further application of Gauss theorem, now in the plane of each face. To this end we consider the orthogonal projection of the point P on the f-th face, say P_f, and assume this point as origin of a local 2D reference frame, see, e.g., Fig. 2.

As reported in [52, 58, 59], we introduce the linear operator $\mathbf{T}_{F_f}$, mapping 2D vectors to 3D ones; the columns of the associated matrix contain the components of two arbitrary 3D unit vectors, e.g., $\mathbf{u}_f$ and $\mathbf{v}_f$, mutually orthogonal and parallel to the generic face F_f

$$\mathbf{T}_{F_f} = \begin{bmatrix} \mathbf{u}_{f1} & \mathbf{v}_{f1} \\ \mathbf{u}_{f2} & \mathbf{v}_{f2} \\ \mathbf{u}_{f3} & \mathbf{v}_{f3} \end{bmatrix} \quad (17)$$

The operator $\mathbf{T}_{F_f}$ is useful to represent the orthogonal decomposition of a generic 3D vector $\mathbf{r}_f$ belonging to F_f; in particular, denoting by d_f the distance of the f-th face from the origin of the reference frame one has

$$\mathbf{r}_f = \mathbf{r}_f^{\parallel} + \mathbf{r}_f^{\perp} = (\mathbf{r}_f\cdot\mathbf{n}_f)\mathbf{n}_f + \mathbf{r}_f^{\parallel} = d_f\mathbf{n}_f + \mathbf{T}_{F_f}\boldsymbol{\rho}_f \quad (18)$$

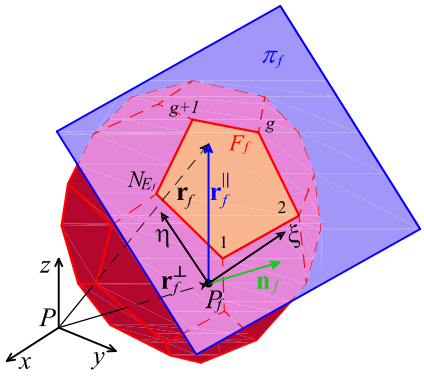

Figure 2: 2D reference frame on the generic face

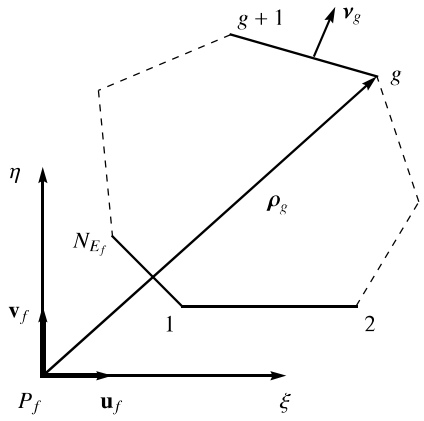

Figure 3: 2D position vector of the g-th vertex of the f-th face

so that $\mathbf{r}_f$ is expressed as sum of a vector $\mathbf{r}_f^{\perp}$ orthogonal to the face F_f and a vector $\mathbf{r}_f^{\parallel}$ parallel to it. In turn the 2D vector $\boldsymbol{\rho}_f$ contains the components of $\mathbf{r}_f^{\parallel}$ in the plane of the face.

Actually, being parallel to F_f, the vector $\mathbf{r}_f^{\parallel}$ can be equivalently expressed as linear combination of two vectors parallel to the face, i.e. the column of $\mathbf{T}_{F_f}$, by means of coordinates representing the 2D vector $\boldsymbol{\rho}_f$.

Multiplying to the left both sides of (18) by $\mathbf{T}_{F_f}^T$, i.e. the transpose of $\mathbf{T}_{F_f}$, one infers

$$\boldsymbol{\rho}_f = \mathbf{T}_{\mathbf{F}_f}^T(\mathbf{r}_f - d_f\mathbf{n}_f) \tag{19}$$

since $\mathbf{T}_{F_f}^T\mathbf{T}_{F_f} = \mathbf{I}_{2D}$ where $\mathbf{I}_{2D}$ is the 2d identity matrix.

The previous relation plays a fundamental role to evaluate the 2D components of the 3D position vectors defining the vertices of the generic face. Actually, the formulas resulting from the two consecutive applications of Gauss theorem are expressed as function of the 2D coordinates of the vertices referred to the cartesian frame local to the face.

In turn, such 2D coordinates need to be computed from the relevant 3D coordinates of the vertices of each face since they represent the basic input data for assigning the polyhedron.

Denoting by $\boldsymbol{\rho}_f = (\xi_f, \eta_f)$ the position vector of each point of the f-th face with respect to P_f and observing that $d_f = \mathbf{r}_f \cdot \mathbf{n}_f$ is constant over each face, the expression $(16)_1$ can be equivalently written as

$$\boldsymbol{\omega}^f = \int_{F_f} \frac{\mathbf{r}_f}{(\mathbf{r}_f \cdot \mathbf{r}_f)^{\frac{3}{2}}} dA_f = \int_{F_f} \frac{\left(d_f\mathbf{n}_f + \mathbf{T}_{F_f}\boldsymbol{\rho}_f\right)}{(\boldsymbol{\rho}_f \cdot \boldsymbol{\rho}_f + d_f^2)^{3/2}} dA_f \tag{20}$$

that is

$$\begin{aligned}\boldsymbol{\omega}^f &= d_f\mathbf{n}_f \int_{F_f} \frac{dA_f}{(\boldsymbol{\rho}_f \cdot \boldsymbol{\rho}_f + d_f^2)^{3/2}} + \\ &+ \mathbf{T}_{F_f} \int_{F_f} \frac{\boldsymbol{\rho}_f}{(\boldsymbol{\rho}_f \cdot \boldsymbol{\rho}_f + d_f^2)^{3/2}} dA_f = \\ &= d_f\mathbf{n}_f\boldsymbol{\kappa}_{F_f} + \mathbf{T}_{F_f}\boldsymbol{\kappa}_{F_f}\end{aligned} \tag{21}$$

where $\boldsymbol{\kappa}_{F_f}$ and $\boldsymbol{\kappa}_{F_f}$ have been evaluated in [52]; their expressions are reported in the Appendix A for the reader's convenience. Expanding $\mathbf{r}_f \otimes \mathbf{r}_f \otimes \mathbf{r}_f$ on account of (18) one has

$$\begin{aligned}\boldsymbol{\Upsilon}^f &= \int_{F_f} \frac{\mathbf{r}_f \otimes \mathbf{r}_f \otimes \mathbf{r}_f}{(\mathbf{r}_f \cdot \mathbf{r}_f)^{5/2}} dA_f = \\ &= d_f^3\mathbf{n}_f \otimes \mathbf{n}_f \otimes \mathbf{n}_f \int_{F_f} \frac{dA_f}{(\boldsymbol{\rho}_f \cdot \boldsymbol{\rho}_f + d_f^2)^{5/2}} + \\ &+ d_f^2\Bigg(\mathbf{T}_{F_f} \int_{F_f} \frac{\boldsymbol{\rho}_f}{(\boldsymbol{\rho}_f \cdot \boldsymbol{\rho}_f + d_f^2)^{5/2}} dA_f \otimes \mathbf{n}_f \otimes \mathbf{n}_f + \\ &+ \mathbf{n}_f \otimes \mathbf{n}_f \otimes \mathbf{T}_{F_f} \int_{F_f} \frac{\boldsymbol{\rho}_f}{(\boldsymbol{\rho}_f \cdot \boldsymbol{\rho}_f + d_f^2)^{5/2}} dA_f + \\ &+ \mathbf{n}_f \otimes \mathbf{T}_{F_f} \int_{F_f} \frac{\boldsymbol{\rho}_f}{(\boldsymbol{\rho}_f \cdot \boldsymbol{\rho}_f + d_f^2)^{5/2}} dA_f \otimes \mathbf{n}_f\Bigg) \\ &+ d_f\Bigg(\mathbf{n}_f \otimes \mathbf{T}_{F_f} \int_{F_f} \frac{\boldsymbol{\rho}_f \otimes \boldsymbol{\rho}_f}{(\boldsymbol{\rho}_f \cdot \boldsymbol{\rho}_f + d_f^2)^{5/2}} dA_f \mathbf{T}_{F_f}^T + \\ &+ \int_{F_f} \frac{\mathbf{T}_{F_f}\boldsymbol{\rho}_f \otimes \mathbf{n}_f \otimes \mathbf{T}_{F_f}\boldsymbol{\rho}_f}{(\boldsymbol{\rho}_f \cdot \boldsymbol{\rho}_f + d_f^2)^{5/2}} dA_f + \\ &+ \mathbf{T}_{F_f} \int_{F_f} \frac{\boldsymbol{\rho}_f \otimes \boldsymbol{\rho}_f}{(\boldsymbol{\rho}_f \cdot \boldsymbol{\rho}_f + d_f^2)^{5/2}} dA_f \mathbf{T}_{F_f}^T \otimes \mathbf{n}_f\Bigg) + \\ &+ \int_{F_f} \frac{\mathbf{T}_{F_f}\boldsymbol{\rho}_f \otimes \mathbf{T}_{F_f}\boldsymbol{\rho}_f \otimes \mathbf{T}_{F_f}\boldsymbol{\rho}_f}{(\boldsymbol{\rho}_f \cdot \boldsymbol{\rho}_f + d_f^2)^{5/2}} dA_f\end{aligned} \tag{22}$$

To make the previous expression more concise we set

$$\varphi_{F_f} = \int_{F_f} \frac{dA_f}{(\boldsymbol{\rho}_f \cdot \boldsymbol{\rho}_f + d_f^2)^{5/2}} \tag{23}$$

$$\boldsymbol{\varphi}_{F_f} = \int_{F_f} \frac{\boldsymbol{\rho}_f}{(\boldsymbol{\rho}_f \cdot \boldsymbol{\rho}_f + d_f^2)^{5/2}} dA_f \tag{24}$$

$$\mathbf{\Phi}_{F_f} = \int_{F_f} \frac{\boldsymbol{\rho}_f \otimes \boldsymbol{\rho}_f}{(\boldsymbol{\rho}_f \cdot \boldsymbol{\rho}_f + d_f^2)^{5/2}} dA_f \tag{25}$$

$$\mathfrak{F}_{F_f} = \int_{F_f} \frac{\boldsymbol{\rho}_f \otimes \boldsymbol{\rho}_f \otimes \boldsymbol{\rho}_f}{(\boldsymbol{\rho}_f \cdot \boldsymbol{\rho}_f + d_f^2)^{5/2}} dA_f \tag{26}$$

and introduce the formal operator $\mathbb{T}_{F_f}^{b...b}$ where the symbol $b...b$ denotes an arbitrary sequence of 0 and 1. In particular

$$\begin{aligned} \mathbb{T}_{F_f}^{11}\mathbf{\Phi}_{F_f} &= \mathbb{T}_{F_f}^{11} \int_{F_f} \frac{\boldsymbol{\rho}_f \otimes \boldsymbol{\rho}_f}{(\boldsymbol{\rho}_f \cdot \boldsymbol{\rho}_f + d_f^2)^{5/2}} dA_f = \\ &= \int_{F_f} \frac{\mathbf{T}_{F_f}\boldsymbol{\rho}_f \otimes \mathbf{T}_{F_f}\boldsymbol{\rho}_f}{(\boldsymbol{\rho}_f \cdot \boldsymbol{\rho}_f + d_f^2)^{5/2}} dA_f = \mathbf{T}_{F_f}\mathbf{\Phi}_{F_f}\mathbf{T}_{F_f}^T \end{aligned} \tag{27}$$

$$\begin{aligned} \mathbb{T}_{F_f}^{111}\mathfrak{F}_{F_f} &= \mathbb{T}_{F_f}^{111} \int_{F_f} \frac{\boldsymbol{\rho}_f \otimes \boldsymbol{\rho}_f \otimes \boldsymbol{\rho}_f}{(\boldsymbol{\rho}_f \cdot \boldsymbol{\rho}_f + d_f^2)^{5/2}} dA_f = \\ &= \int_{F_f} \frac{\mathbf{T}_{F_f}\boldsymbol{\rho}_f \otimes \mathbf{T}_{F_f}\boldsymbol{\rho}_f \otimes \mathbf{T}_{F_f}\boldsymbol{\rho}_f}{(\boldsymbol{\rho}_f \cdot \boldsymbol{\rho}_f + d_f^2)^{5/2}} dA_f \end{aligned} \tag{28}$$

so that

$$\begin{aligned} \mathbf{\Upsilon}^f &= d_f^3 \varphi_{F_f} \mathbf{n}_f \otimes \mathbf{n}_f \otimes \mathbf{n}_f + \\ &+ d_f^2 \Big[\left(\mathbf{T}_{F_f}\boldsymbol{\varphi}_{F_f}\right) \otimes \mathbf{n}_f \otimes \mathbf{n}_f + \mathbf{n}_f \otimes \mathbf{n}_f \otimes \left(\mathbf{T}_{F_f}\boldsymbol{\varphi}_{F_f}\right) + \\ &+ \mathbf{n}_f \otimes \left(\mathbf{T}_{F_f}\boldsymbol{\varphi}_{F_f}\right) \otimes \mathbf{n}_f \Big] + \\ &+ d_f \Big[\mathbf{n}_f \otimes \mathbf{T}_{F_f}\mathbf{\Phi}_{F_f}\mathbf{T}_{F_f}^T + \mathbb{T}_{F_f}^{101}\left(\mathbf{\Phi}_{F_f} \wedge \mathbf{n}_f\right) + \\ &+ \mathbf{T}_{F_f}\mathbf{\Phi}_{F_f}\mathbf{T}_{F_f}^T \otimes \mathbf{n}_f \Big] + \mathbb{T}_{F_f}^{111}\mathfrak{F}_{F_f} \end{aligned} \tag{29}$$

where

$$\mathbf{\Phi}_{F_f} \wedge \mathbf{n}_f = \int_{F_f} \frac{\boldsymbol{\rho}_f \otimes \mathbf{n}_f \otimes \boldsymbol{\rho}_f}{(\boldsymbol{\rho}_f \cdot \boldsymbol{\rho}_f + d_f^2)^{5/2}} dA_f \tag{30}$$

Notice the previous symbol is purely formal since it involves the tensor product od 2D and 3D vectors. It has been deliberately introduced to focus the reader's attention on the fact that one first evaluates the integral (25) as a tensor product of 2D vectors, as detailed in the sequel; only subsequently the resulting formula is expressed in terms of 3D vectors, by means of the operator $\mathbf{T}_{F_f}$, and combined with the 3D vector $\mathbf{n}_f$.

The analytical evaluation of the face integrals (23) - (26) will be detailed in the next section.

4. Analytical expression of the face integrals in terms of 1D integrals

Aim of this section is to illustrate how to express the integrals (23) - (26) in terms of 1D integrals extended to the edges defining the boundary $\partial\Omega_f$ of each face. To this end we shall make repeatedly use of the Gauss theorem in several of its variants depending on the field to integrate.

4.1. Analytical evaluation of the integral φ_{F_f} in terms of 1D integrals

To evaluate the integral φ_{F_f} in (23) we invoke a general result exploited in [49, 60] concerning the properties of the vector field $\boldsymbol{\rho}_f/(\boldsymbol{\rho}_f \cdot \boldsymbol{\rho}_f)$. Actually, given a continuous function ψ, it turns out to be

$$\mathrm{div}\left[\frac{\boldsymbol{\rho}_f}{\boldsymbol{\rho}_f \cdot \boldsymbol{\rho}_f}\right] = 0 \quad \text{if } \boldsymbol{\rho}_f \neq \mathbf{o} \tag{31}$$

and

$$\int_F \psi(\boldsymbol{\rho}) \mathrm{div}\left[\frac{\boldsymbol{\rho}_f}{\boldsymbol{\rho}_f \cdot \boldsymbol{\rho}_f}\right] dA = \begin{cases} 0 & \text{if } \mathbf{o} \notin F \\ \alpha(\mathbf{o})\psi(\mathbf{o}) & \text{if } \mathbf{o} \in F \end{cases} \tag{32}$$

where F is an arbitrary two-dimensional domain and $\alpha(\mathbf{o})$ represents the angular measure, expressed in radians, of the intersection between F and a circular neighborhood of the singularitiy point $\boldsymbol{\rho} = \mathbf{o}$, see [51, 61] for details and [55, 62] for further applications. In particular $\alpha(\mathbf{o}) = 2\pi$ if $\mathbf{o}$ belongs to the interior of F and $\alpha(\mathbf{o}) = \pi$ if $\mathbf{o}$ belongs to a straight edge defining the boundary ∂F of F.

Notice that when $\mathbf{o} \in F$ the integral on the left-hand side above is simply obtained by sampling the value of the function ψ at $\mathbf{o}$ scaled by the quantity $\alpha(\mathbf{o})$.

We can now evaluate the integral (23) by invoking the differential identity

$$\mathrm{div}(\psi\mathbf{u}) = \mathrm{grad}\psi \cdot \mathbf{u} + \psi\, \mathrm{div}\mathbf{u} \tag{33}$$

where ψ ($\mathbf{u}$) is a scalar (vector) field.

In particular, one has

$$\begin{aligned} &\mathrm{div}\left[\left(\boldsymbol{\rho}_f \cdot \boldsymbol{\rho}_f + d_f^2\right)^{-3/2} \frac{\boldsymbol{\rho}_f}{\boldsymbol{\rho}_f \cdot \boldsymbol{\rho}_f}\right] = \\ &= -\frac{3}{2}\frac{2\boldsymbol{\rho}_f}{\left(\boldsymbol{\rho}_f \cdot \boldsymbol{\rho}_f + d_f^2\right)^{5/2}} \cdot \frac{\boldsymbol{\rho}_f}{\boldsymbol{\rho}_f \cdot \boldsymbol{\rho}_f} + \\ &\quad + \frac{1}{\left(\boldsymbol{\rho}_f \cdot \boldsymbol{\rho}_f + d_f^2\right)^{3/2}} \mathrm{div}\frac{\boldsymbol{\rho}_f}{\boldsymbol{\rho}_f \cdot \boldsymbol{\rho}_f} = \\ &= -\frac{3}{\left(\boldsymbol{\rho}_f \cdot \boldsymbol{\rho}_f + d_f^2\right)^{5/2}} + \\ &\quad + \frac{1}{\left(\boldsymbol{\rho}_f \cdot \boldsymbol{\rho}_f + d_f^2\right)^{3/2}} \mathrm{div}\frac{\boldsymbol{\rho}_f}{\boldsymbol{\rho}_f \cdot \boldsymbol{\rho}_f} \end{aligned} \tag{34}$$

Integrating over F_f and invoking (32), the application of Gauss theorem to the integral on the left-hand side above yields

$$\begin{aligned} \varphi_{F_f} &= \int_{F_f} \frac{dA_f}{(\boldsymbol{\rho}_f \cdot \boldsymbol{\rho}_f + d_f^2)^{5/2}} = \\ &= -\frac{1}{3}\int_{\partial F_f} \frac{\boldsymbol{\rho}_f \cdot \boldsymbol{\nu}}{(\boldsymbol{\rho}_f \cdot \boldsymbol{\rho}_f)(\boldsymbol{\rho}_f \cdot \boldsymbol{\rho}_f + d_f^2)^{3/2}} ds_f + \frac{1}{3}\frac{\alpha_f}{|d_f|^3} = \\ &= -\frac{1}{3}\varphi_{\partial F_f} + \frac{1}{3}\frac{\alpha_f}{|d_f|^3} \end{aligned} \tag{35}$$

where $\boldsymbol{\nu}$ is the 2D outward unit normal to ∂F_f and $\alpha_f = \alpha(\mathbf{o}_f)$ is different from zero if and only if the point $\boldsymbol{\rho}_f = \mathbf{o}$ belongs to F_f.

4.2. Analytical evaluation of the integral $\boldsymbol{\varphi}_{F_f}$ in terms of 1D integrals

The integral $\boldsymbol{\varphi}_{F_f}$ in (24) can be simply expressed in terms of line integrals by observing that

$$\operatorname{grad}\left[\left(\boldsymbol{\rho}_f \cdot \boldsymbol{\rho}_f + d_f^2\right)^{-3/2}\right] = -\frac{3\boldsymbol{\rho}_f}{\left(\boldsymbol{\rho}_f \cdot \boldsymbol{\rho}_f + d_f^2\right)^{5/2}} \tag{36}$$

Thus application of Gauss theorem yields

$$\begin{aligned}\boldsymbol{\varphi}_{F_f} &= \int_{F_f} \frac{\boldsymbol{\rho}_f}{(\boldsymbol{\rho}_f \cdot \boldsymbol{\rho}_f + d_f^2)^{5/2}} dA_f = \\ &= -\frac{1}{3}\int_{\partial F_f} \frac{\boldsymbol{\nu}}{(\boldsymbol{\rho}_f \cdot \boldsymbol{\rho}_f + d_f^2)^{3/2}} ds_f = -\frac{1}{3}\boldsymbol{\varphi}_{\partial F_f}\end{aligned} \tag{37}$$

4.3. Analytical evaluation of the integral $\boldsymbol{\Phi}_{F_f}$ in terms of 1D integrals

The evaluation of the integral $\boldsymbol{\Phi}_{F_f}$ in (25) by means of line integrals is based on the differential dentity

$$\operatorname{grad}(\psi\,\mathbf{u}) = \mathbf{u} \otimes \operatorname{grad}\psi + \psi\,\operatorname{grad}\mathbf{u} \tag{38}$$

to the product $\left(\boldsymbol{\rho}_f \cdot \boldsymbol{\rho}_f + d_f^2\right)^{-3/2}\boldsymbol{\rho}_f$. Actually, one has

$$\begin{aligned}&\operatorname{grad}\left[(\boldsymbol{\rho}_f \cdot \boldsymbol{\rho}_f + d_f^2)^{-3/2}\boldsymbol{\rho}_f\right] = \\ &= \boldsymbol{\rho}_f \otimes \left[-\frac{3}{2}\frac{2\boldsymbol{\rho}_f}{\left(\boldsymbol{\rho}_f \cdot \boldsymbol{\rho}_f + d_f^2\right)^{5/2}}\right] + \frac{\mathbf{I}_{2D}}{\left(\boldsymbol{\rho}_f \cdot \boldsymbol{\rho}_f + d_f^2\right)^{3/2}} = \\ &= -\frac{3\boldsymbol{\rho}_f \otimes \boldsymbol{\rho}_f}{\left(\boldsymbol{\rho}_f \cdot \boldsymbol{\rho}_f + d_f^2\right)^{5/2}} + \frac{\mathbf{I}_{2D}}{\left(\boldsymbol{\rho}_f \cdot \boldsymbol{\rho}_f + d_f^2\right)^{3/2}}\end{aligned} \tag{39}$$

where $\mathbf{I}_{2D}$ is the two-dimensional identity operator.

Integrating the previous expression over F_f and invoking the following variant of the Gauss theorem

$$\int_{F_f} \operatorname{grad}\mathbf{u}\, dA = \int_{\partial F_f} \mathbf{u} \otimes \boldsymbol{\nu}\, dA \tag{40}$$

one has

$$\begin{aligned}\boldsymbol{\Phi}_{F_f} &= \int_{F_f} \frac{\boldsymbol{\rho}_f \otimes \boldsymbol{\rho}_f}{(\boldsymbol{\rho}_f \cdot \boldsymbol{\rho}_f + d_f^2)^{5/2}} dA_f = \\ &= -\frac{1}{3}\int_{\partial F_f} \frac{\boldsymbol{\rho}_f \otimes \boldsymbol{\nu}}{(\boldsymbol{\rho}_f \cdot \boldsymbol{\rho}_f + d_f^2)^{3/2}} ds_f + \\ &\quad + \frac{\mathbf{I}_{2D}}{3}\int_{F_f} \frac{\boldsymbol{\rho}_f}{(\boldsymbol{\rho}_f \cdot \boldsymbol{\rho}_f + d_f^2)^{3/2}} dA_f = \\ &= -\frac{1}{3}\int_{\partial F_f} \frac{\boldsymbol{\rho}_f \otimes \boldsymbol{\nu}}{(\boldsymbol{\rho}_f \cdot \boldsymbol{\rho}_f + d_f^2)^{3/2}} ds_f + \frac{\mathbf{I}_{2D}}{3}\boldsymbol{\kappa}_{F_f}\end{aligned} \tag{41}$$

The evaluation of the last integral is detailed in the Appendix A.

4.4. Analytical evaluation of the integral $\mathfrak{F}_{F_f}$ in terms of 1D integrals

The express the integral $\mathfrak{F}_{F_f}$ in (26) by means of line integrals we need to invoke the differential dentity

$$\begin{aligned}\left[\operatorname{grad}(\psi\,\mathbf{a}\otimes\mathbf{b})\right]_{/ijh} &= (\psi\, a_i b_j)_{/h} = \\ &= a_i b_j \psi_{/h} + \psi\, a_{i/h} b_j + \psi\, a_i b_{j/h} = \\ &= \mathbf{a}\otimes\mathbf{b}\otimes\operatorname{grad}\psi + \psi\,\operatorname{grad}\mathbf{a}\boxtimes\mathbf{b} + \\ &\quad + \psi\,\mathbf{a}\otimes\operatorname{grad}\mathbf{b}\end{aligned} \tag{42}$$

involving scalar (ψ) and vector ($\mathbf{a}$, $\mathbf{b}$) fields. The symbol $\boxtimes$ used to combine the rank-two tensor $\operatorname{grad}\mathbf{a}$ and the vector $\mathbf{b}$ is defined as a suitable extension of the more classical tensor product ($\mathbf{A}\boxtimes\mathbf{B}$) between rank-two tensors [63]

$$(\mathbf{A}\boxtimes\mathbf{B})\,\mathbf{C} = \mathbf{A}\mathbf{C}\mathbf{B}^T \tag{43}$$

or, in components

$$(\mathbf{A}\boxtimes\mathbf{B})_{ijhk} = A_{ih}\,B_{jk} \tag{44}$$

In particular we define

$$(\mathbf{A}\boxtimes\mathbf{b})\,\mathbf{c} = \mathbf{A}\mathbf{c}\otimes\mathbf{b} \quad \forall\,\mathbf{A},\,\mathbf{b},\,\mathbf{c} \tag{45}$$

or, in components

$$(\mathbf{A}\boxtimes\mathbf{b})_{ijh} = A_{ih}\,b_j \tag{46}$$

Actually

$$[(\mathbf{A}\boxtimes\mathbf{b})\,\mathbf{c}]_{ij} = (\mathbf{A}\boxtimes\mathbf{b})_{ijh}\,c_h \tag{47}$$

yields

$$[(\mathbf{A}\boxtimes\mathbf{b})\,\mathbf{c}]_{ij} = (\mathbf{A}\,\mathbf{c}\otimes\mathbf{b})_{ij} = A_{ih}\,c_h\,b_j = A_{ih}\,b_j\,c_h \tag{48}$$

by invoking the definition (45).

Thus, applying formula (42)

$$\begin{aligned}&\operatorname{grad}\left[(\boldsymbol{\rho}_f \cdot \boldsymbol{\rho}_f + d_f^2)^{-3/2}\boldsymbol{\rho}_f\otimes\boldsymbol{\rho}_f\right] = \\ &= \boldsymbol{\rho}_f\otimes\boldsymbol{\rho}_f\otimes\left[-\frac{3}{2}\frac{2\boldsymbol{\rho}_f}{(\boldsymbol{\rho}_f \cdot \boldsymbol{\rho}_f + d_f^2)^{5/2}}\right] + \\ &\quad + \frac{\mathbf{I}_{2D}\boxtimes\boldsymbol{\rho}_f}{(\boldsymbol{\rho}_f \cdot \boldsymbol{\rho}_f + d_f^2)^{3/2}} + \frac{\boldsymbol{\rho}_f\otimes\mathbf{I}_{2D}}{(\boldsymbol{\rho}_f \cdot \boldsymbol{\rho}_f + d_f^2)^{3/2}}\end{aligned} \tag{49}$$

so that being

$$\begin{aligned}&\int_{F_f} \operatorname{grad}\left[(\boldsymbol{\rho}_f \cdot \boldsymbol{\rho}_f + d_f^2)^{-3/2}\boldsymbol{\rho}_f\otimes\boldsymbol{\rho}_f\right] dA = \\ &= \int_{\partial F_f} \frac{\boldsymbol{\rho}_f\otimes\boldsymbol{\rho}_f\otimes\boldsymbol{\nu}}{(\boldsymbol{\rho}_f \cdot \boldsymbol{\rho}_f + d_f^2)^{3/2}} ds_f\end{aligned} \tag{50}$$

application of the Gauss theorem to (49) yields

$$\begin{aligned}\mathfrak{F}_{F_f} &= \int_{F_f} \frac{\boldsymbol{\rho}_f \otimes \boldsymbol{\rho}_f \otimes \boldsymbol{\rho}_f}{(\boldsymbol{\rho}_f \cdot \boldsymbol{\rho}_f + d_f^2)^{5/2}} dA_f = \\ &= -\frac{1}{3} \int_{\partial F_f} \frac{\boldsymbol{\rho}_f \otimes \boldsymbol{\rho}_f \otimes \boldsymbol{\nu}}{(\boldsymbol{\rho}_f \cdot \boldsymbol{\rho}_f + d_f^2)^{3/2}} ds_f + \\ &+ \frac{\mathbf{I}_{2D}}{3} \boxtimes \int_{F_f} \frac{\boldsymbol{\rho}_f}{(\boldsymbol{\rho}_f \cdot \boldsymbol{\rho}_f + d_f^2)^{3/2}} dA_f + \\ &+ \int_{F_f} \frac{\boldsymbol{\rho}_f}{(\boldsymbol{\rho}_f \cdot \boldsymbol{\rho}_f + d_f^2)^{3/2}} dA_f \otimes \frac{\mathbf{I}_{2D}}{3} = \\ &= -\frac{1}{3} \mathfrak{F}_{\partial F_f} + \frac{\mathbf{I}_{2D}}{3} \boxtimes \boldsymbol{\kappa}_{F_f} + \boldsymbol{\kappa}_{F_f} \otimes \frac{\mathbf{I}_{2D}}{3}\end{aligned} \tag{51}$$

5. Algebraic expression of the face integrals in terms of 2D vectors

At this stage we despose of analytical expressions of the face integrals as line integrals extended to the boundary of each face. The relevant expressions are provided by eqn. (35) for $\boldsymbol{\varphi}_{F_f}$, eqn. (37) for $\boldsymbol{\varphi}_{F_f}$, eqn. (41) for $\boldsymbol{\Phi}_{F_f}$ and eqn. (51) for $\mathfrak{F}_{F_f}$. Having supposed that each face of the inclusion is polygonal, the previous line integrals can be given an algebraic expression depending upon the 2D position vectors of the vertices; in particular it is assumed that these are numbered in consecutive order by circulating along the boundary ∂F_f of the generic face in a counter-clockwise sense with respect to the outward unit normal $\mathbf{n}_f$.

Supposing that the generic g-th side of ∂F_f is identified by the two position vertices $\boldsymbol{\rho}_g$ and $\boldsymbol{\rho}_{g+1}$, its parametric equation is given by

$$\boldsymbol{\rho}(\lambda_g) = \boldsymbol{\rho}_g + \lambda_g(\boldsymbol{\rho}_{g+1} - \boldsymbol{\rho}_g) = \boldsymbol{\rho}_g + \lambda_g \Delta\boldsymbol{\rho}_g \tag{52}$$

where $\lambda_g \in [0,\ 1]$ is a local abscissa along the g-th side.

Of future use is also the expression of the outward unit vector $\boldsymbol{\nu}_g$ orthogonal to the g-th side, given by

$$\boldsymbol{\nu}_g = \frac{\boldsymbol{\rho}_{g+1}^{\perp} - \boldsymbol{\rho}_g^{\perp}}{|\boldsymbol{\rho}_{g+1} - \boldsymbol{\rho}_g|} = \frac{\Delta\boldsymbol{\rho}_g^{\perp}}{l_g} \tag{53}$$

where $l_g = |\mathbf{r}_{g+1} - \mathbf{r}_g|$ is the length of each edge and $(\cdot)^{\perp}$ represents the clock-wise rotation of $(\cdot)$ by $\pi/2$.

Additional quantities repeatedly used in the sequel are

$$\begin{aligned}\boldsymbol{\rho}(\lambda_g) \cdot \boldsymbol{\rho}(\lambda_g) &= (\boldsymbol{\rho}_g + \lambda_g \Delta\boldsymbol{\rho}_g) \cdot (\boldsymbol{\rho}_g + \lambda_g \Delta\boldsymbol{\rho}_g) = \\ &= \boldsymbol{\rho}_g \cdot \boldsymbol{\rho}_g + 2(\boldsymbol{\rho}_g \cdot \Delta\boldsymbol{\rho}_g)\lambda_g + (\Delta\boldsymbol{\rho}_g \cdot \Delta\boldsymbol{\rho}_g)\lambda_g^2 = \\ &= u_g + 2q_g\lambda_g + p_g\lambda_g^2 = P_u(\lambda_g)\end{aligned} \tag{54}$$

and

$$\begin{aligned}\boldsymbol{\rho}(\lambda_g) \cdot \Delta\boldsymbol{\rho}_g^{\perp} &= (\boldsymbol{\rho}_g + \lambda_g \Delta\boldsymbol{\rho}_g) \cdot \Delta\boldsymbol{\rho}_g^{\perp} = \\ &= \boldsymbol{\rho}_g \cdot \Delta\boldsymbol{\rho}_g^{\perp} + \Delta\boldsymbol{\rho}_g \cdot \Delta\boldsymbol{\rho}_g^{\perp}\lambda_g = \left(\boldsymbol{\rho}_g \cdot \boldsymbol{\rho}_{g+1}^{\perp}\right)\lambda_g\end{aligned} \tag{55}$$

we shall also set $w_g = u_g + d_f^2$ and $P_w(\lambda_g) = p_g\lambda_g^2 + 2q_g\lambda_g + w_g = P_u(\lambda_g) + d_f^2$

Setting $\boldsymbol{\rho}_{g+1} = (\xi_{g+1},\ \eta_{g+1})$ we have denoted by $\boldsymbol{\rho}_{g+1}^{\perp}$ the quantity defined by $(\eta_{g+1},\ -\xi_{g+1})$.

5.1. Algebraic expression of the face integral $\boldsymbol{\varphi}_{F_f}$ in terms of 2D vectors

Invoking formulas (52), (53), (54), (55) and (35) the integral $\boldsymbol{\varphi}_{\partial F_f}$ can be evaluated analytically as follows

$$\begin{aligned}\boldsymbol{\varphi}_{\partial F_f} &= \int_{\partial F_f} \frac{\boldsymbol{\rho}_f \cdot \boldsymbol{\nu}}{(\boldsymbol{\rho}_f \cdot \boldsymbol{\rho}_f)(\boldsymbol{\rho}_f \cdot \boldsymbol{\rho}_f + d_f^2)^{3/2}} ds_f = \\ &= \sum_{g=1}^{N_{Ef}} \int_{l_g} \frac{\boldsymbol{\rho}_f \cdot \boldsymbol{\nu}_g}{(\boldsymbol{\rho}_f \cdot \boldsymbol{\rho}_f)(\boldsymbol{\rho}_f \cdot \boldsymbol{\rho}_f + d_f^2)^{3/2}} ds_g \\ &= \sum_{g=1}^{N_{Ef}} \int_{l_g} \frac{\boldsymbol{\rho}_f(\lambda_g) \cdot \boldsymbol{\nu}_g}{\left[\boldsymbol{\rho}_f(\lambda_g) \cdot \boldsymbol{\rho}_f(\lambda_g)\right]\left[\boldsymbol{\rho}_f(\lambda_g) \cdot \boldsymbol{\rho}_f(\lambda_g) + d_f^2\right]^{3/2}} d\lambda_g\end{aligned} \tag{56}$$

where N_{Ef} is the number of edges of the face F_f, $\boldsymbol{\nu}_g$ is the outward unit normal to the g-th edge and $ds_g = l_g\, d\lambda_g$.

Recalling (53), (54) and (55) one has

$$\begin{aligned}\boldsymbol{\varphi}_{\partial F_f} &= \sum_{g=1}^{N_{Ef}} \int_0^1 \frac{\boldsymbol{\rho}_f(\lambda_g) \cdot \Delta\boldsymbol{\rho}_g^{\perp}}{\left[\boldsymbol{\rho}_f(\lambda_g) \cdot \boldsymbol{\rho}_f(\lambda_g)\right]\left[\boldsymbol{\rho}_f(\lambda_g) \cdot \boldsymbol{\rho}_f(\lambda_g) + d_f^2\right]^{3/2}} d\lambda_g \\ &= \sum_{g=1}^{N_{Ef}} \left(\boldsymbol{\rho}_g \cdot \boldsymbol{\rho}_{g+1}^{\perp}\right) \int_0^1 \frac{d\lambda_g}{P_u(\lambda_g)\left[P_w(\lambda_g)\right]^{3/2}} = \\ &= \sum_{g=1}^{N_{Ef}} \left(\boldsymbol{\rho}_g \cdot \boldsymbol{\rho}_{g+1}^{\perp}\right) I_{4g}\end{aligned} \tag{57}$$

where the explicit expression of the integral I_{4g} is detailed in the Appendix B.

In conclusion, on account of (35) one has

$$\boldsymbol{\varphi}_{F_f} = \frac{1}{3}\frac{\alpha_f}{|d_f|^3} - \frac{1}{3}\sum_{g=1}^{N_{Ef}} \left(\boldsymbol{\rho}_g \cdot \boldsymbol{\rho}_{g+1}^{\perp}\right) I_{4g} \tag{58}$$

that represents the final result.

5.2. Algebraic expression of the face integral $\boldsymbol{\varphi}_{F_f}$ in terms of 2D vectors

Invoking formulas (52), (53), (54), (55) and (37) the integral $\boldsymbol{\varphi}_{F_f}$ admits the following analytical expression

$$\begin{aligned}\boldsymbol{\varphi}_{\partial F_f} &= \int_{\partial F_f} \frac{\boldsymbol{\nu}}{(\boldsymbol{\rho}_f \cdot \boldsymbol{\rho}_f + d_f^2)^{3/2}} ds_f = \\ &= \sum_{g=1}^{N_{Ef}} \int_{l_g} \frac{\boldsymbol{\nu}_g}{(\boldsymbol{\rho}_f \cdot \boldsymbol{\rho}_f + d_f^2)^{3/2}} ds_g = \\ &= \sum_{g=1}^{N_{Ef}} \Delta\boldsymbol{\rho}_g^{\perp} \int_0^1 \frac{d\lambda_g}{\left[P_w(\lambda_g)\right]^{3/2}} = \sum_{g=1}^{N_{Ef}} \Delta\boldsymbol{\rho}_g^{\perp} I_{0g}\end{aligned} \tag{59}$$

yielding finally

$$\boldsymbol{\varphi}_{F_f} = \int_{F_f} \frac{\boldsymbol{\rho}_f}{(\boldsymbol{\rho}_f \cdot \boldsymbol{\rho}_f + d_f^2)^{5/2}} dA_f = -\frac{1}{3} \sum_{g=1}^{N_{Ef}} \Delta\boldsymbol{\rho}_g^{\perp} I_{0g} \tag{60}$$

where the integral I_{0g} is analytically evaluated in the Appendix A.

5.3. Algebraic expression of the face integral $\boldsymbol{\Phi}_{F_f}$ in terms of 2D vectors

By following the same path of reasoning illustrated in the previous subsection, the integral $\boldsymbol{\Phi}_{\partial F_f}$ in formula (41) can be transformed as follows

$$\begin{aligned} \boldsymbol{\Phi}_{\partial F_f} &= \int_{\partial F_f} \frac{\boldsymbol{\rho}_f \otimes \boldsymbol{\nu}}{(\boldsymbol{\rho}_f \cdot \boldsymbol{\rho}_f + d_f^2)^{3/2}} ds_f = \\ &= \sum_{g=1}^{N_{Ef}} \int_{l_g} \frac{\boldsymbol{\rho}_f}{(\boldsymbol{\rho}_f \cdot \boldsymbol{\rho}_f + d_f^2)^{3/2}} ds_g \otimes \boldsymbol{\nu}_g \end{aligned} \tag{61}$$

or equivalently

$$\begin{aligned} \boldsymbol{\Phi}_{\partial F_f} &= \sum_{g=1}^{N_{Ef}} \left\{ \int_0^1 \frac{\boldsymbol{\rho}_g}{\left[P_w(\lambda_g)\right]^{3/2}} d\lambda_g + \int_0^1 \frac{\Delta\boldsymbol{\rho}_g \lambda_g}{\left[P_w(\lambda_g)\right]^{3/2}} d\lambda_g \right\} \otimes \Delta\boldsymbol{\rho}_g^{\perp} \\ &= \sum_{g=1}^{N_{Ef}} \left[\boldsymbol{\rho}_g I_{0g} + \Delta\boldsymbol{\rho}_g I_{1g} \right] \otimes \Delta\boldsymbol{\rho}_g^{\perp} \end{aligned} \tag{62}$$

where the integrals I_{0g} and I_{1g} are analytically evaluated in the Appendix A. Thus, are finally has

$$\boldsymbol{\Phi}_{F_f} = \frac{\mathbf{I}_{2D}}{3} \boldsymbol{\kappa}_{F_f} - \frac{1}{3} \sum_{g=1}^{N_{Ef}} \left[\boldsymbol{\rho}_g I_{0g} + \Delta\boldsymbol{\rho}_g I_{1g} \right] \otimes \Delta\boldsymbol{\rho}_g^{\perp} \tag{63}$$

on account of (41).

5.4. Algebraic expression of the face integral $\mathfrak{F}_{F_f}$ in terms of 2D vectors

It remains to transform the integral $\mathfrak{F}_{\partial F_f}$ in (51). Proceeding as in the previous subsections we set

$$\begin{aligned} \mathfrak{F}_{\partial F_f} &= \int_{\partial F_f} \frac{\boldsymbol{\rho}_f \otimes \boldsymbol{\rho}_f \otimes \boldsymbol{\nu}}{(\boldsymbol{\rho}_f \cdot \boldsymbol{\rho}_f + d_f^2)^{3/2}} ds_f = \\ &= \sum_{g=1}^{N_{Ef}} \int_{l_g} \frac{\boldsymbol{\rho}_f \otimes \boldsymbol{\rho}_f}{(\boldsymbol{\rho}_f \cdot \boldsymbol{\rho}_f + d_f^2)^{3/2}} ds_g \otimes \boldsymbol{\nu}_g = \\ &= \sum_{g=1}^{N_{Ef}} \left[\int_0^1 \frac{\boldsymbol{\rho}(\lambda_g) \otimes \boldsymbol{\rho}(\lambda_g) d\lambda_g}{\left[P_w(\lambda_g)\right]^{3/2}} \right] \otimes \Delta\boldsymbol{\rho}_g^{\perp} \end{aligned} \tag{64}$$

Being

$$\begin{aligned} \boldsymbol{\rho}(\lambda_g) \otimes \boldsymbol{\rho}(\lambda_g) &= (\boldsymbol{\rho}_g + \lambda_g \Delta\boldsymbol{\rho}_g) \otimes (\boldsymbol{\rho}_g + \lambda_g \Delta\boldsymbol{\rho}_g) = \\ &= \boldsymbol{\rho}_g \otimes \boldsymbol{\rho}_g + \lambda_g \left(\boldsymbol{\rho}_g \otimes \Delta\boldsymbol{\rho}_g + \Delta\boldsymbol{\rho}_g \otimes \boldsymbol{\rho}_g \right) + \\ &\quad + \lambda_g^2 \Delta\boldsymbol{\rho}_g \otimes \Delta\boldsymbol{\rho}_g = \\ &= \mathbf{D}_{\boldsymbol{\rho}_g \boldsymbol{\rho}_g} + \lambda_g \mathbf{D}_{\boldsymbol{\rho}_g \Delta\boldsymbol{\rho}_g} + \lambda_g^2 \mathbf{D}_{\Delta\boldsymbol{\rho}_g \Delta\boldsymbol{\rho}_g} \end{aligned} \tag{65}$$

we finally have

$$\begin{aligned} \mathfrak{F}_{\partial F_f} &= \sum_{g=1}^{N_{Ef}} \left\{ \mathbf{D}_{\boldsymbol{\rho}_g \boldsymbol{\rho}_g} \int_0^1 \frac{d\lambda_g}{\left[P_w(\lambda_g)\right]^{3/2}} + \right. \\ &\quad + \mathbf{D}_{\boldsymbol{\rho}_g \Delta\boldsymbol{\rho}_g} \int_0^1 \frac{\lambda_g d\lambda_g}{\left[P_w(\lambda_g)\right]^{3/2}} + \\ &\quad \left. + \mathbf{D}_{\Delta\boldsymbol{\rho}_g \Delta\boldsymbol{\rho}_g} \int_0^1 \frac{\lambda_g^2 d\lambda_g}{\left[P_w(\lambda_g)\right]^{3/2}} \right\} \otimes \Delta\boldsymbol{\rho}_g^{\perp} = \\ &= \sum_{g=1}^{N_{Ef}} \left\{ I_{0g} \mathbf{D}_{\boldsymbol{\rho}_g \boldsymbol{\rho}_g} + I_{1g} \mathbf{D}_{\boldsymbol{\rho}_g \Delta\boldsymbol{\rho}_g} + I_{2g} \mathbf{D}_{\Delta\boldsymbol{\rho}_g \Delta\boldsymbol{\rho}_g} \right\} \otimes \Delta\boldsymbol{\rho}_g^{\perp} \end{aligned} \tag{66}$$

so that

$$\begin{aligned} \mathfrak{F}_{F_f} &= \frac{\mathbf{I}_{2D}}{3} \boxtimes \boldsymbol{\kappa}_{F_f} + \boldsymbol{\kappa}_{F_f} \otimes \frac{\mathbf{I}_{2D}}{3} - \\ &\quad - \frac{1}{3} \sum_{g=1}^{N_{Ef}} \left\{ I_{0g} \mathbf{D}_{\boldsymbol{\rho}_g \boldsymbol{\rho}_g} + I_{1g} \mathbf{D}_{\boldsymbol{\rho}_g \Delta\boldsymbol{\rho}_g} + I_{2g} \mathbf{D}_{\Delta\boldsymbol{\rho}_g \Delta\boldsymbol{\rho}_g} \right\} \otimes \Delta\boldsymbol{\rho}_g^{\perp} \end{aligned} \tag{67}$$

where the integrals I_{0g}, I_{1g} e I_{2g}, are evaluated in the Appendix A.

6. Algebraic expression of the face integrals in terms of 3D vectors

The integrals evaluated in the previous section have been expressed as function of 2D vectors collecting the coordinates of the vertices of the inclusion projected in the plane of each face.

However the tensors $\boldsymbol{\omega}^f$ and $\boldsymbol{\Upsilon}^f$ are expressed in terms of 3D vectors so that the formulas derived in the previous section need to be suitably reformulated in terms of the 3D coordinates of each vertex.

This does not represent a problem for the expression (21) of $\boldsymbol{\omega}^f$ since it is already expressed in this form. The same does occur for the quantities $\mathbf{T}_{F_f} \boldsymbol{\varphi}_{F_f}$ and $\mathbf{T}_{F_f} \boldsymbol{\Phi}_{F_f} \mathbf{T}_{F_f}^T$ appearing in formula (29) for $\boldsymbol{\Upsilon}^f$. Thus, we just need to detail how to express the rank-three tensors $\mathbb{T}_{F_f}^{101}(\boldsymbol{\Phi}_{F_f} \wedge \mathbf{n}_f)$ and $\mathbb{T}_{F_f}^{111} \mathfrak{F}_{F_f}$ as a function of 3D vectors.

To this end setting

$$\mathbf{G}_f = \mathbf{T}_{F_f} \boldsymbol{\Phi}_{F_f} \mathbf{T}_{F_f}^T \tag{68}$$

we have

$$\mathbb{T}^{101}\left(\boldsymbol{\Phi}_{F_f} \wedge \mathbf{n}_f \right) = \int_{F_f} \frac{\mathbf{T}_{F_f} \boldsymbol{\rho}_f \otimes \mathbf{n}_f \otimes \mathbf{T}_{F_f} \boldsymbol{\rho}_f}{(\boldsymbol{\rho}_f \cdot \boldsymbol{\rho}_f + d_f^2)^{3/2}} dA_f = \mathbf{G}_f \otimes_{23} \mathbf{n}_f \tag{69}$$

where $\otimes_{23}$ denotes the tensor product obtained by switching the second and third index of the rank-three tensor $\mathbf{G}_f \otimes \mathbf{n}_f$.

To address the case of the tensor $\mathbb{T}_{F_f}^{111} \mathfrak{F}_{F_f}$ we first notice that, according to (67), the tensor $\mathfrak{F}_{F_f}$ is expressed as a sum of rank-three tensors, two of which are given by tensor product between

rank-two tensors and a vector, while the remaining ones are given by the tensor product of three 2D vectors. Denoting be $\boldsymbol{\gamma}$, $\boldsymbol{\delta}$ and $\boldsymbol{\varepsilon}$ the factors of these last addends of $\mathfrak{F}_{F_f}$, one trivially has

$$\mathbb{T}^{111}\left(\boldsymbol{\gamma}\otimes\boldsymbol{\delta}\otimes\boldsymbol{\varepsilon}\right)=\mathbf{T}_{F_f}\boldsymbol{\gamma}\otimes\mathbf{T}_{F_f}\boldsymbol{\delta}\otimes\mathbf{T}_{F_f}\boldsymbol{\varepsilon}=\mathbf{t}\otimes\mathbf{v}\otimes\mathbf{w} \tag{70}$$

so that the tensor product above between 3D vectors can be suitably expressed in matrix form. For istance one can set

$$[\mathbf{Z}]=\begin{bmatrix} v_1w_1 & v_1w_2 & v_1w_3 \\ v_2w_1 & v_2w_2 & v_2w_3 \\ v_3w_1 & v_3w_2 & v_3w_3 \end{bmatrix} \tag{71}$$

and

$$\left[\mathbf{t}\otimes\mathbf{v}\otimes\mathbf{w}\right]=\begin{bmatrix} t_1\,[\mathbf{Z}] \\ t_2\,[\mathbf{Z}] \\ t_3\,[\mathbf{Z}] \end{bmatrix} \tag{72}$$

and define in accordance the composition of rank-three tensors with vectors and rank-two tensors. Finally it is straightforward to check that

$$\begin{aligned}\mathbb{T}^{111}\left(\mathbf{I}_{2D}\boxtimes\boldsymbol{\kappa}_{F_f}\right)&=\mathbf{T}_{F_f}\mathbf{I}_{2D}\mathbf{T}_{F_f}^{T}\boxtimes\mathbf{T}_{F_f}\boldsymbol{\kappa}_{F_f}=\\&=\mathbf{I}_{3D}\boxtimes\left(\mathbf{T}_{F_f}\boldsymbol{\kappa}_{F_f}\right)\end{aligned} \tag{73}$$

and

$$\mathbb{T}^{111}\left(\boldsymbol{\kappa}_{F_f}\otimes\mathbf{I}_{2D}\right)=\left(\mathbf{T}_{F_f}\boldsymbol{\kappa}_{F_f}\right)\otimes\mathbf{I}_{3D} \tag{74}$$

that can expressed in matrix form similarly to (72).

7. Numerical examples

We report hereafter the results of some numerical examples in order to show the effectiveness of the proposed approach and the robustness of the relevant implementation in a Matlab code.

The compiled version of the code can be downloaded at the address specified in the Appendix B.

7.1. Preliminary validation of the Matlab Code

In ordere to carry out a prliminary validation of the code, the Eshelby tensor has been evaluated for a spherical inclusion since the following analytical expression is available for the tensor in Voigt notation

$$\tilde{S}=\begin{bmatrix} \frac{1}{15}\frac{7-5\nu}{1-\nu} & \frac{1}{15}\frac{5\nu-1}{1-\nu} & \frac{1}{15}\frac{5\nu-1}{1-\nu} & 0 & 0 & 0 \\ \frac{1}{15}\frac{5\nu-1}{1-\nu} & \frac{1}{15}\frac{7-5\nu}{1-\nu} & \frac{1}{15}\frac{5\nu-1}{1-\nu} & 0 & 0 & 0 \\ \frac{1}{15}\frac{5\nu-1}{1-\nu} & \frac{1}{15}\frac{5\nu-1}{1-\nu} & \frac{1}{15}\frac{7-5\nu}{1-\nu} & 0 & 0 & 0 \\ 0 & 0 & 0 & \frac{2}{15}\frac{4-5\nu}{1-\nu} & 0 & 0 \\ 0 & 0 & 0 & 0 & \frac{2}{15}\frac{4-5\nu}{1-\nu} & 0 \\ 0 & 0 & 0 & 0 & 0 & \frac{2}{15}\frac{4-5\nu}{1-\nu} \end{bmatrix} \tag{75}$$

where ν is the Poisson's ratio. In particular the tensor is indipendent from the dimension of the inclusion and constant within the inclusion.

Assuming $\nu = 0.3$ the following expression is arrived at

$$\mathbb{S}=\begin{bmatrix} 0.5238 & 0.0476 & 0.0476 & 0 & 0 & 0 \\ 0.0476 & 0.5238 & 0.0476 & 0 & 0 & 0 \\ 0.0476 & 0.0476 & 0.5238 & 0 & 0 & 0 \\ 0 & 0 & 0 & 0.4762 & 0 & 0 \\ 0 & 0 & 0 & 0 & 0.4762 & 0 \\ 0 & 0 & 0 & 0 & 0 & 0.4762 \end{bmatrix} \tag{76}$$

The Eshelby tensor $\mathbb{S}$ has been numerically evaluated by approximating the sphere with triangular facets obtained by considering n equally spaced parallel and meridian planes, see, e.g., fig. 4 for the case $n = 20$. The following results, obtained for

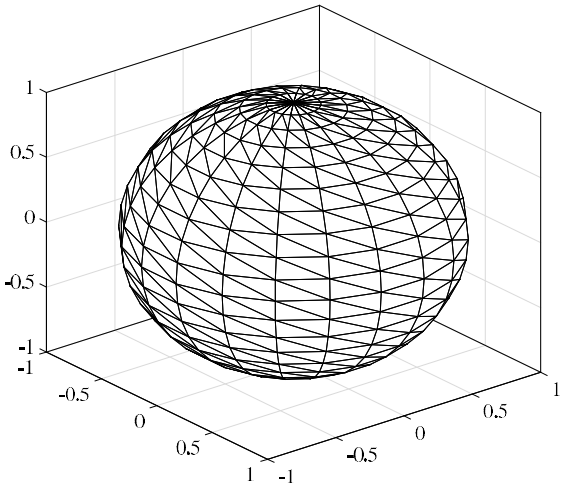

Figure 4: Polyhedral approximation of the sphere obtained by considering $n = 20$ equally spaced parallel and meridian planes

$n = 10$,

$$\mathbb{S}_{10}=\begin{bmatrix} 0.5291 & 0.0477 & 0.0505 & 0 & 0 & 0 \\ 0.0477 & 0.5291 & 0.0505 & 0 & 0 & 0 \\ 0.0447 & 0.0447 & 0.5131 & 0 & 0 & 0 \\ 0 & 0 & 0 & 0.4814 & 0 & 0 \\ 0 & 0 & 0 & 0 & 0.4736 & 0 \\ 0 & 0 & 0 & 0 & 0 & 0.4736 \end{bmatrix} \tag{77}$$

$n = 20$,

$$\mathbb{S}_{20}=\begin{bmatrix} 0.5251 & 0.0476 & 0.0483 & 0 & 0 & 0 \\ 0.0476 & 0.5251 & 0.0483 & 0 & 0 & 0 \\ 0.0469 & 0.0469 & 0.5212 & 0 & 0 & 0 \\ 0 & 0 & 0 & 0.4775 & 0 & 0 \\ 0 & 0 & 0 & 0 & 0.4755 & 0 \\ 0 & 0 & 0 & 0 & 0 & 0.4755 \end{bmatrix} \tag{78}$$

and $n = 40$,

$$\mathbb{S}_{40}=\begin{bmatrix} 0.5241 & 0.0476 & 0.0478 & 0 & 0 & 0 \\ 0.0476 & 0.5241 & 0.0478 & 0 & 0 & 0 \\ 0.0474 & 0.0474 & 0.5231 & 0 & 0 & 0 \\ 0 & 0 & 0 & 0.4765 & 0 & 0 \\ 0 & 0 & 0 & 0 & 0.4760 & 0 \\ 0 & 0 & 0 & 0 & 0 & 0.4760 \end{bmatrix} \tag{79}$$

clearly show how the numerical solution tends to the analytical one as n increases.

7.2. Comparison with the results reported in [56]

More demanding benchmark tests of the proposed approach have been obtained by considering three of the examples addressed by Gao and Liu [56] with reference to a cuboidal, an octahedral and a tetradecahedral inclusion.

These are particularly interesting examples since some descrepancies with the results reported in [56] have obliged us to further validate our approach by supplementing the analytical evaluation of the integrals addressed in the previous sections with a numerical one.

7.2.1. Inclusion of cuboidal shape

Let us consider a cuboidal inclusion immersed in an infinite elastic space characterized by a Poisson's ratio $\nu = 0.3$, see, e.g., fig. 5. The side length of the cube is equal to 2 and the origin of the cartesian reference frame coincides with the barycenter of the cube.

The Eshelby tensor is computed at points P having x_1 coordinated ranging from to 0 and 2, i.e. symmetrically with respect to the face orthogonal to x_1 axis. Clearly, due to the symmetry of the inclusion, the results presented in the sequel do apply as well to points P placed along the x_2 and x_3 axes.

The components S_{1111} and S_{1212} of the Eshelby tensor, plotted in figs. 6, and 12 respectively, have been computed in Gao et al., while the additional components in (14) have not. For this reason the analytical computation of the components have been supplemented with a numerical one obtained by numerically integrating the face integrals $\boldsymbol{\omega}^f$ and $\boldsymbol{\Upsilon}^f$ in formula (16).

Notice that the point P at which the components of the Eshelby tensor are computed is internal to the inclusion for $0 \leq x_1 < 1$, external to it for $1 < x_1 \leq 2$ and belongs to its boundary for $x_1 = 1$.

Furthermore all the components, with the exception of S_{2222}, S_{3333} and S_{2233} are discontinuous at the boundary of the inclusion.

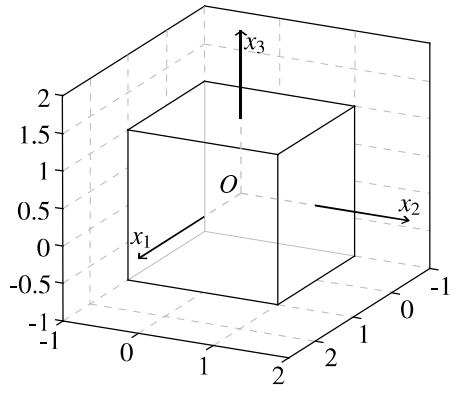

Figure 5: A cuboidal inclusion having edge length equal to 2.

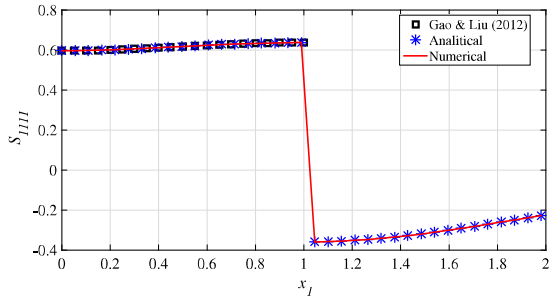

Figure 6: Component S_{1111} of the Eshelby tensor relevant to the cuboidal inclusion of fig. 5 at points P placed along the x_1 axis.

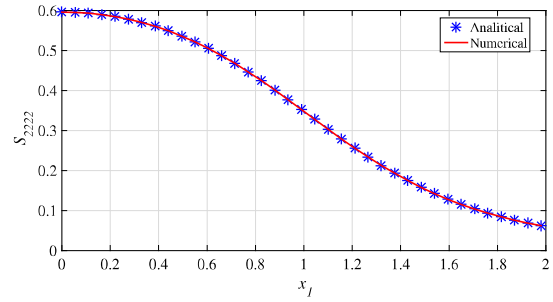

Figure 7: Component S_{2222} of the Eshelby tensor relevant to the cuboidal inclusion of fig. 5 at points P placed along the x_1 axis.

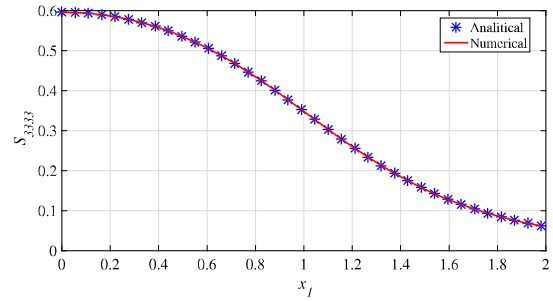

Figure 8: Component S_{3333} of the Eshelby tensor relevant to the cuboidal inclusion of fig. 5 at points P placed along the x_1 axis.

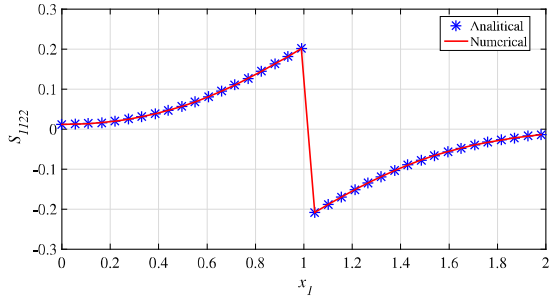

Figure 9: Component S_{1122} of the Eshelby tensor relevant to the cuboidal inclusion of fig. 5 at points P placed along the x_1 axis.

7.2.2. Inclusion of octahedral shape

We now consider an octahedral inclusion belonging to an infinite elastic space having a Poisson's ratio $\nu = 0.3$, see, e.g.,

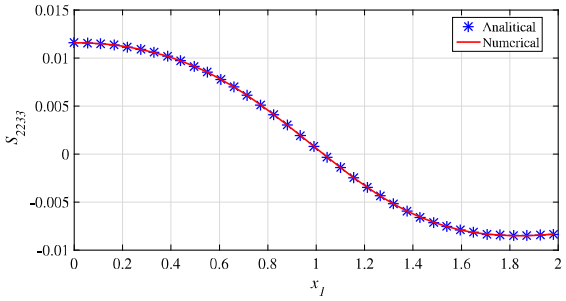

Figure 10: Component S_{2233} of the Eshelby tensor relevant to the cuboidal inclusion of fig. 5 at points P placed along the x_1 axis.

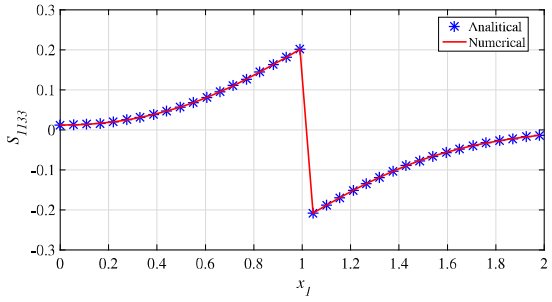

Figure 11: Component S_{1133} of the Eshelby tensor relevant to the cuboidal inclusion of fig. 5 at points P placed along the x_1 axis.

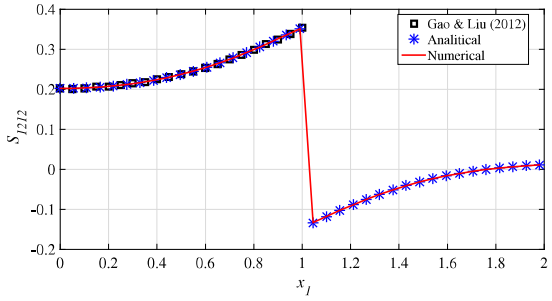

Figure 12: Component S_{1212} of the Eshelby tensor relevant to the cuboidal inclusion of fig. 5 at points P placed along the x_1 axis.

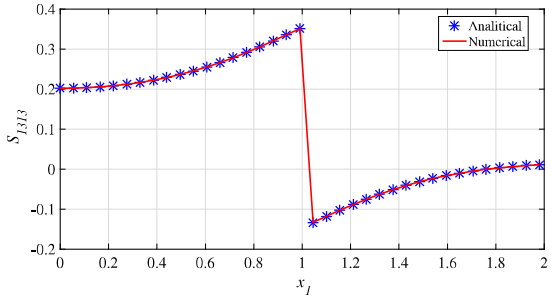

Figure 13: Component S_{1313} of the Eshelby tensor relevant to the cuboidal inclusion of fig. 5 at points P placed along the x_1 axis.

fig. 15. The edge length of the octahedron is equal to 2 and the barycenter coincides with the origin of the reference frame.

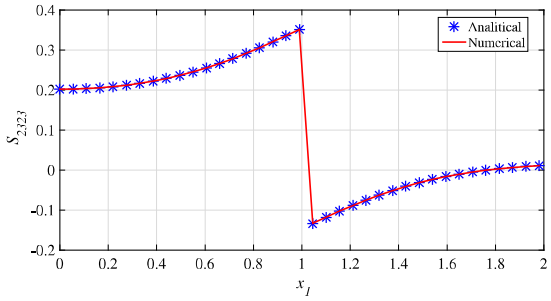

Figure 14: Component S_{2323} of the Eshelby tensor relevant to the cuboidal inclusion of fig. 5 at points P placed along the x_1 axis.

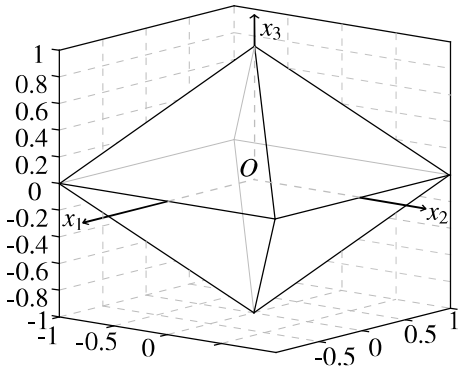

Figure 15: An octahedral inclusion havinhg edge length equal to 2.

The point P at which the Eshelby tensor is evaluated can be anywhere between $x_1 = 0$, i.e. at the barycenter of the inclusion, and $x_1 = 2$, i.e. outside the inclusion. The components of $\mathbb{S}$ are plotted in figs. 16-24 but only for S_{1111} and S_{1212} it has been possible to make a comparison with the values contributed by Gao and Liu [56], though experiencing some discrepancies.

For this reason, as well as for validating the analytical formulas contributed in the previous sections, we have numerically integrated the face integrals $\boldsymbol{\omega}^f$ and $\boldsymbol{\Upsilon}^f$ in formula (16).

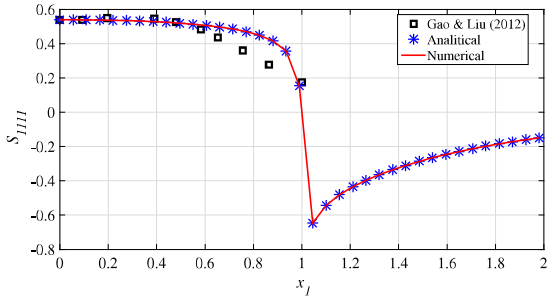

Figure 16: Component S_{1111} of the Eshelby tensor relevant to the octahedral inclusion of fig. 15 at points P placed along the x_1 axis.

7.3. Inclusion of tetrakaidecahedral shape

A tetrakaidecahedron can be generated by uniformly truncating the six corners of an octahedron and is known to be the only

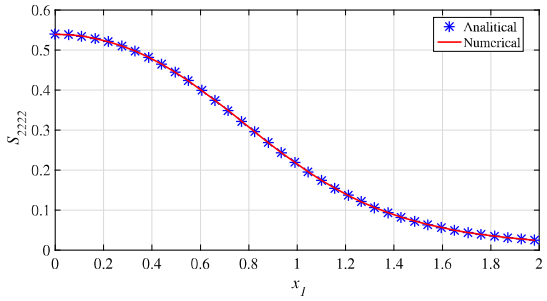

Figure 17: Component S_{2222} of the Eshelby tensor relevant to the octahedral inclusion of fig. 15 at points P placed along the x_1 axis.

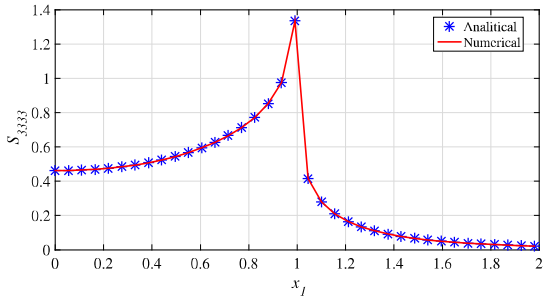

Figure 18: Component S_{3333} of the Eshelby tensor relevant to the octahedral inclusion of fig. 15 at points P placed along the x_1 axis.

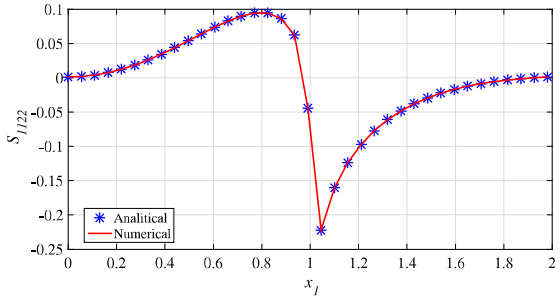

Figure 19: Component S_{1122} of the Eshelby tensor relevant to the octahedral inclusion of fig. 15 at points P placed along the x_1 axis.

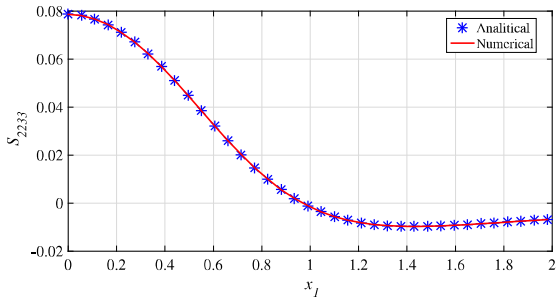

Figure 20: Component S_{2233} of the Eshelby tensor relevant to the octahedral inclusion of fig. 15 at points P placed along the x_1 axis.

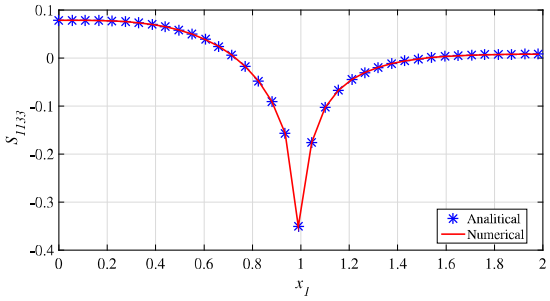

Figure 21: Component S_{1133} of the Eshelby tensor relevant to the octahedral inclusion of fig. 15 at points P placed along the x_1 axis.

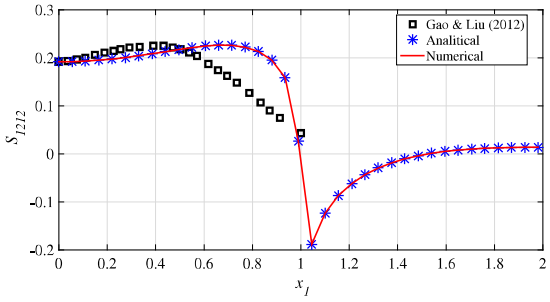

Figure 22: Component S_{1212} of the Eshelby tensor relevant to the octahedral inclusion of fig. 15 at points P placed along the x_1 axis.

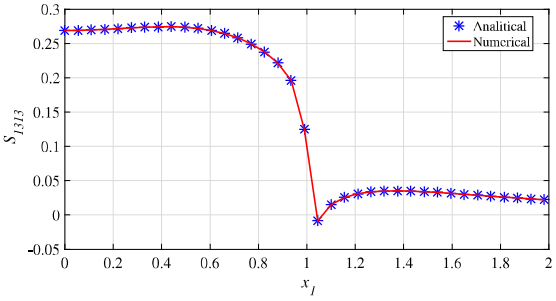

Figure 23: Component S_{1313} of the Eshelby tensor relevant to the octahedral inclusion of fig. 15 at points P placed along the x_1 axis.

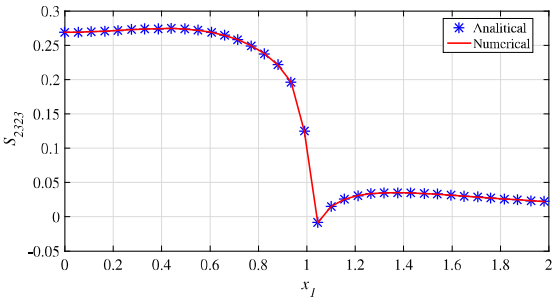

Figure 24: Component S_{2323} of the Eshelby tensor relevant to the octahedral inclusion of fig. 15 at points P placed along the x_1 axis.

polyhedron that can pack with identical units to fill space and nearly minimize the surface energy. In particular we consider the tetrakaidecahedron illustrated in fig. 25. The barycenter of the inclusion coincides with the origin of the reference frame

and the components of the Eshelby tensor have been evaluated at points P placed along the x_1 axis in the range $0 \leq x_1 \leq 2$.

A comparison with the analogous results contributed by Gao and Liu [56] has been possible only for the components S_{1111} and S_{1212}, see, e.g., figs. 26 and 32, though some differences can be noticed for values x_1 ranging in the interval $[0.8\,,1]$.

For this reason we have further validated our Matlab code by comparing the analytical results, associated with the formulation detailed in the previous section, with the numerical ones obtained by quadrature of the face integrals $\boldsymbol{\omega}^f$ and $\boldsymbol{\Upsilon}^f$ reported in formula (16).

As it can be seen from fig. 26-34 a perfect agreement between analytical and numerical evaluation of the Eshelby tensor is obtained.

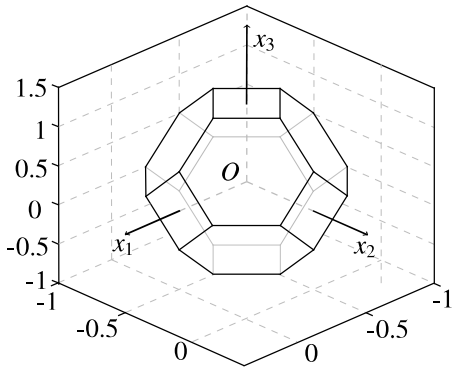

Figure 25: A tetrakaidecahedral inclusion having distance between vertices opposite with respect to the barycenter equal to 2.

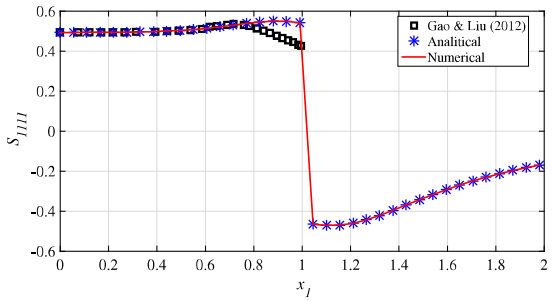

Figure 26: Component S_{1111} of the Eshelby tensor relevant to the tetrakaidecahedral inclusion of fig. 25 at points P placed along the x_1 axis.

8. Conclusions

We have derived an analytical expression of the Eshelby tensor field for arbitrary polyhedral inclusions by converting its original expression, containing 3D integrals extended to the domain of the inclusion, to 2D ones extended to the relevant boundary. The result has been obtained by exploiting recent results on Newtonian potential [52, 53], based upon a generalized version of the Gauss theorem which suitably takes into account the singularities of the fields to be integrated.

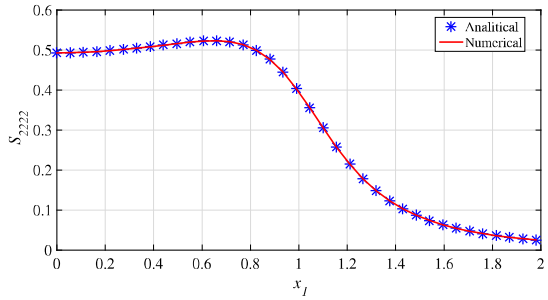

Figure 27: Component S_{2222} of the Eshelby tensor relevant to the tetrakaidecahedral inclusion of fig. 25 at points P placed along the x_1 axis.

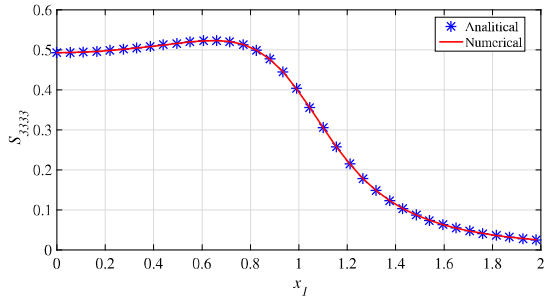

Figure 28: Component S_{3333} of the Eshelby tensor relevant to the tetrakaidecahedral inclusion of fig. 25 at points P placed along the x_1 axis.

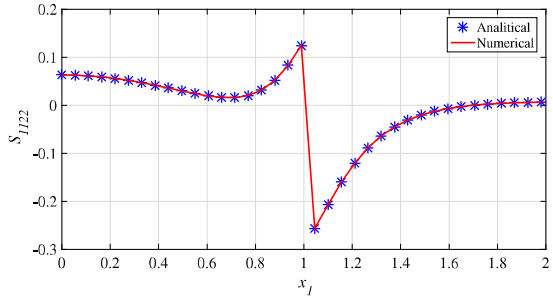

Figure 29: Component S_{1122} of the Eshelby tensor relevant to the tetrakaidecahedral inclusion of fig. 25 at points P placed along the x_1 axis.

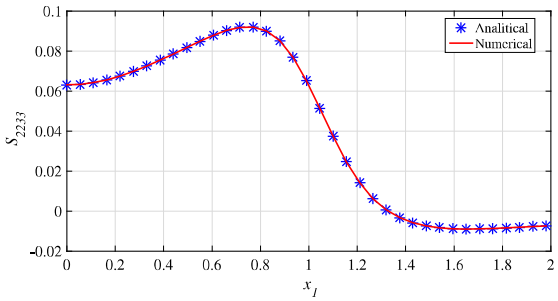

Figure 30: Component S_{2233} of the Eshelby tensor relevant to the tetrakaidecahedral inclusion of fig. 25 at points P placed along the x_1 axis.

A further application of the Gauss theorem has allowed us to further reduce the face integrals, i.e. the 2D integrals extended

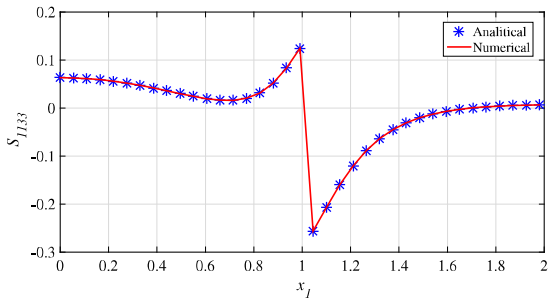

Figure 31: Component S_{1133} of the Eshelby tensor relevant to the tetrakaidecahedral inclusion of fig. 25 at points P placed along the x_1 axis.

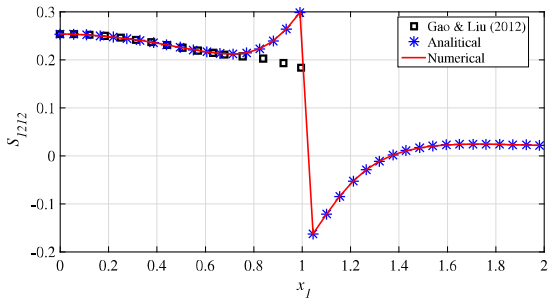

Figure 32: Component S_{1212} of the Eshelby tensor relevant to the tetrakaidecahedral inclusion of fig. 25 at points P placed along the x_1 axis.

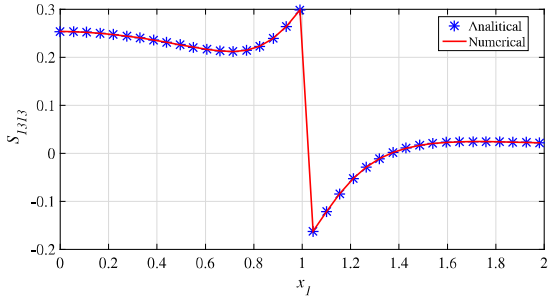

Figure 33: Component S_{1313} of the Eshelby tensor relevant to the tetrakaidecahedral inclusion of fig. 25 at points P placed along the x_1 axis.

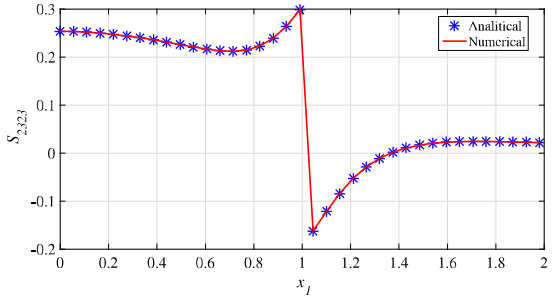

Figure 34: Component S_{2323} of the Eshelby tensor relevant to the tetrakaidecahedral inclusion of fig. 25 at points P placed along the x_1 axis.

to the faces of the inclusion, to simpler 1D integrals extended to the edges of each face.

Analytical integration of such line integrals has ultimately allowed us to derive an algebraic expression of the Eshelby tensor that is directly expressed as function of the position vectors defining the vertices of the polyhedron.

The extension of the proposed approach to the case of non-uniform eigenstrain within the inclusion will be dealt with in forthcoming papers.

References

[1] A. Mortensen, Concise Encyclopedia of Composite Materials, Amsterdam, Netherlands, 2007.

[2] J. D. Eshelby, Elastic inclusions and inhomogeneities, Progress in solid mechanics **2** (1) (1961) 89–140.

[3] T. Mura, Micromechanics of defects in solids, Martinus Nijhoff, 1982.

[4] H. S. Kim, J.-U. Jang, J. Yu, S. Y. Kim, Thermal conductivity of polymer composites based on the length of multi-walled carbon nanotubes, Composites Part B: Engineering **79** (2015) 505–512.

[5] L. Ma, A. M. Korsunsky, The principle of equivalent eigenstrain for inhomogeneous inclusion problems, International Journal of Solids and Structures **51** (25) (2014) 4477–4484.

[6] A. G. Khachaturyan, Theory of structural transformations in solids, Dover, 2013.

[7] T. Sabiston, M. Mohammadi, M. Cherkaoui, J. Lvesque, K. Inal, Micromechanics based elasto-visco-plastic response of long fibre composites using functionally graded interphases at quasi-static and moderate strain rates, Composites Part B: Engineering **100** (2016) 31 – 43.

[8] R. Sankaran, C. Laird, Deformation field of a misfitting inclusion, Journal of the Mechanics and Physics of Solids **24** (4) (1976) 251–262.

[9] D. Bimberg, M. Grundmann, N. N. Ledentsov, Quantum dot heterostructures, New York: Wiley, 1998.

[10] J. D. Eshelby, The determination of the elastic field of an ellipsoidal inclusion, and related problems., Proceedings of the The Royal Society of London A: Mathematical, Physical and Engineering Sciences **241** (1226) (1957) 376–396.

[11] T. Mura, H.M., Shodja, Y. Hirose, Inclusion problems, Applied Mechanics Reviews **49** (1996) S118–S127.

[12] T. Mura, Inclusion problems, Applied Mechanics Reviews **41** (1998) 15–20.

[13] N. Charalambakis, Homogenization techniques and micromechanics, A survey and perspectives. Applied Mechanics Reviews **63** (2010) 030803–030810.

[14] I. Ovid'ko, A. Sheinerman, Elastic fields of inclusions in nanocomposite solids, Reviews on Advanced Materials Science **9** (2005) 17–33.

[15] Nemat-Nasser, S., M. Hori, Micromechanics: overall properties of heterogeneous materials, 2nd Edition, Academic Press, Elsevier, 1999.

[16] J. Qu, M. Cherkaoui, Fundamentals of micromechanics of solids, Hoboken, NJ: Wiley, 2006.

[17] S. Li, G. Wang, Introduction to micromechanics and nanomechanics, Singapore: World Scientific, 2008.

[18] J. Aboudi, S. M. Arnold, B. A. Bednarcyk, Micromechanics of composite materials - A generalized multiscale analysis approach, Butterworth-Heinemann, 2013.

[19] G. J. Dvorak, Micromechanics of composite materials, Springer, 2013.

[20] V. Buryachenko, Micromechanics of heterogeneous materials, 1st Edition, Springer, 2007.

[21] Z. X. Guo, Multiscale materials modelling: fundamentals and applications, Elsevier, 2007.

[22] G. A. Pavliotis, A. Stuart, Multiscale methods: averaging and homogenization, Springer, 2008.

[23] C. C. Mei, B. Vernescu, Homogenization methods for multiscale mechanics, World Scientific, 2010.

[24] T. Mori, K. Tanaka, Average stress in matrix and average elastic energy of materials with misfitting inclusions, Acta Metal Mater **21** (1973) 571–574.

[25] A. Caporale, L. Feo, R. Luciano, Damage mechanics of cement concrete modeled as a four-phase composite, Composites Part B: Engineering **65** (2014) 124 – 130.

[26] A. Caporale, L. Feo, R. Luciano, Eigenstrain and Fourier series for evaluation of elastic local fields and effective properties of periodic composites, Composites Part B: Engineering **81** (2015) 251 – 258.
[27] M. Talò, B. Krause, J. Pionteck, G. Lanzara, W. Lacarbonara, An updated micromechanical model based on morphological characterization of carbon nanotube nanocomposites, Composites Part B: Engineering **115** (2017) 70 – 78.
[28] E. García-Macías, L. Rodriguez-Tembleque, R. Castro-Triguero, A. Sáez, Buckling analysis of functionally graded carbon nanotube-reinforced curved panels under axial compression and shear, Composites Part B: Engineering **108** (2017) 243 – 256.
[29] B. Sobhaniaragh, M. Nejati, W. J. Mansur, Buckling modelling of ring and stringer stiffened cylindrical shells aggregated by graded CNTs, Composites Part B: Engineering **124** (2017) 120 – 133.
[30] E. García-Macías, L. Rodríguez-Tembleque, R. Castro-Triguero, A. Sáez, Eshelby-Mori-Tanaka approach for post-buckling analysis of axially compressed functionally graded CNT/polymer composite cylindrical panels, Composites Part B: Engineering **128** (2017) 208 – 224.
[31] W. Azoti, A. Elmarakbi, Constitutive modelling of ductile damage matrix reinforced by platelets-like particles with imperfect interfaces: Application to graphene polymer nanocomposite materials, Composites Part B: Engineering **113** (2017) 55 – 64.
[32] Y. Koutsawa, Multi-coating inhomogeneities approach for composite materials with temperature-dependent constituents under small strain and finite thermal perturbation assumptions, Composites Part B: Engineering **112** (2017) 137 – 147.
[33] B. Sobhaniaragh, R. C. Batra, W. J. Mansur, F. C. Peters, Thermal response of ceramic matrix nanocomposite cylindrical shells using Eshelby-Mori-Tanaka homogenization scheme, Composites Part B: Engineering **118** (2017) 41 – 53.
[34] D. H. Sung, K. Myungsoo, Y. B. Park, Prediction of thermal conductivities of carbon-containing fiber-reinforced and multiscale hybrid composites, Composites Part B: Engineering **133** (2018) 232 – 239.
[35] H. M. Shodja, B. Alemi, Effective shear modulus of solids reinforced by randomly oriented-/aligned-elliptic nanofibers in couple stress elasticity, Composites Part B: Engineering **117** (2017) 150 – 164.
[36] M. Majewski, M. Kursa, P. Holobut, K. Kowalczyk-Gajewska, Micromechanical and numerical analysis of packing and size effects in elastic particulate composites, Composites Part B: Engineering **124** (2017) 158 – 174.
[37] Q. Zhou, X. Jin, Z. Wang, J. Wang, L. M. Keer, Q. Wang, Numerical implementation of the equivalent inclusion method for 2d arbitrarily shaped inhomogeneities, Journal of Elasticity **118** (1) (2015) 39–61.
[38] P. Harrison, Quantum Wells, Wires and Dots: Theoretical and Computational Physics, 1999.
[39] G. J. Rodin, Eshelby's inclusion problem for polygons and polyhedra, Journal of the Mechanics and Physics of Solids **44** (12) (1996) 1977–1995.
[40] J. Waldvogel, The Newtonian potential of homogeneous polyhedra, Zeitschrift für Angewandte Mathematik und Physik ZAMP **30** (2) (1979) 388–398.
[41] H. Nozaki, M. Taya, Elastic fields in a polygon-shaped inclusion with uniform eigenstrains, Journal of Applied Mechanics **64** (3) (1997) 495–502.
[42] H. Nozaki, M. Taya, Elastic fields in a polyhedral inclusion with uniform eigenstrains and related problems, Journal of Applied Mechanics **68** (3) (2001) 441–452.
[43] C. Q. Ru, Analytic solution for Eshelby's problem of an inclusion of arbitrary shape in a plane or half-plane, Journal of Applied Mechanics **66** (2) (1999) 315–322.
[44] M. Huang, W. Zou, Q. S. Zheng, Explicit expression of Eshelby tensor for arbitrary weakly non-circular inclusion in two-dimensional elasticity, International Journal of Engineering Science **47** (11) (2009) 1240–1250.
[45] W. Zou, Q. He, M. Huang, Q. Zheng, Eshelby's problem of non-elliptical inclusions, Journal of the Mechanics and Physics of Solids **58** (3) (2010) 346–372.
[46] Q. S. Zheng, Z. H. Zhao, D. X. Du, Irreducible structure, symmetry and average of Eshelby's tensor fields in isotropic elasticity, Journal of the Mechanics and Physics of Solids **54** (2) (2006) 368–383.
[47] S. Trotta, F. Marmo, L. Rosati, Analytical expression of the Eshelby tensor for arbitrary polygonal inclusions in two-dimensional elasticity, Composites Part B: Engineering **106** (2016) 48 – 58.
[48] S. Trotta, F. Marmo, L. Rosati, Evaluation of the Eshelby tensor for polygonal inclusions, Composites Part B: Engineering **115** (2017) 170–181.
[49] M. G. D'Urso, Some Remark on the Computation of the Gravitational Potential of Masses with Linearly Varying Density, VIII Hotine–Marussi International Symposium on Mathematical Geodesy. Springer, Berlin, Heidelberg, 2016.
[50] M. G. D'Urso, S. Trotta, Comparative assessment of linear and bilinear prism-based strategies for terrain correction computations, Journal of Geodesy **89** (3) (2015) 199–215.
[51] M. G. D'Urso, The gravity anomaly of a 2D polygonal body having density contrast given by polynomial functions, Surveys in Geophysics **36** (3) (2015) 391–425.
[52] M. G. D'Urso, S. Trotta, Gravity anomaly of polyhedral bodies having a polinomial density contrast, Survey in Geophysics **38** (4) (2017) 781–832.
[53] M. G. D'Urso, F. Marmo, On a generalized Love's problem, Computers & Geosciences **61** (2013) 144–151.
[54] S. Sessa, M. G. D'Urso, Employment of Bayesian networks for risk assessment of excavation processes in dense urban areas, In: Proceedings of the 11th international conference (ICOSSAR 2013) 30163–30169.
[55] L. Rosati, F. Marmo, Closed-form expressions of the thermo-mechanical fields induced by a uniform heat source acting over an isotropic half-space, International Journal of Heat and Mass Transfer **75** (2014) 272–283.
[56] X. L. Gao, M. Q. Liu, Strain gradient solution for the Eshelby-type polyhedral inclusion problem, Journal of the Mechanics and Physics of Solids **60** (2) (2012) 261–276.
[57] M. Huang, P. Wu, G. Guan, W. Liu, Explicit expressions of the Eshelby tensor for an arbitrary 3d weakly non-spherical inclusion, Acta Mechanica **217** (1-2) (2011) 17–38.
[58] F. Marmo, L. Rosati, A general approach to the solution of Boussinesq's problem for polynomial pressures acting over polygonal domains, Journal of Elasticity **122** (2016) 75–112.
[59] F. Marmo, S. Sessa, L. Rosati, Analytical solution of the Cerruti problem under linearly distributed horizontal pressures over polygonal domains, Journal of Elasticity **124** (2016) 27–56.
[60] F. Marmo, F. Toraldo, L. Rosati, Analytical formulas and design charts for transversely isotropic half-spaces subject to linearly distributed pressures, Meccanica **51** (2016) 2909–2928.
[61] F. Marmo, F. Toraldo, L. Rosati, Transversely isotropic half-spaces subject to surface pressures, International Journal of Solids and Structures (2017) 104–105, 35–49.
[62] F. Marmo, F. Toraldo, A. Rosati, L. Rosati, Numerical solution of smooth and rough contact problems, Accepted for publication in Meccanica.
[63] L. Rosati, Derivatives and Rates of the Stretch and Rotation Tensors, Journal of Elasticity **56** (3) (1999) 213–230.
[64] F. Chen, A. Giraud, I. Sevostianov, D. Grgic, Numerical evaluation of the Eshelby tensor for a concave superspherical inclusion, International Journal of Engineering Science **93** (2015) 51–58.

Appendix A.

We hereby report the expressions of the integrals κ_{F_f} and $\boldsymbol{\kappa}_{F_f}$ referred to in formula (21) and some definite integrals used throughout the paper. To this end we remind that for a generic edge g of the face F_f, parameterized by the end vectors $\boldsymbol{\rho}_g$ and $\boldsymbol{\rho}_{g+1}$ collecting the coordinates of the vertices in the $2D$ reference frame local to F_f, we have set $\Delta\boldsymbol{\rho}_g = \boldsymbol{\rho}_{g+1} - \boldsymbol{\rho}_g$

$$u_g = \boldsymbol{\rho}_g \cdot \boldsymbol{\rho}_g \quad q_g = \boldsymbol{\rho}_g \cdot \Delta\boldsymbol{\rho}_g \quad p_g = \Delta\boldsymbol{\rho}_g \cdot \Delta\boldsymbol{\rho}_g \tag{A.1}$$

and $w_g = u_g + d_f^2$. We further introduce the quantities

$$ATN1_g = \arctan \frac{|d_f|(p_g + q_g)}{\sqrt{p_g u_g - q_g^2}\sqrt{p_g + 2q_g + w_g}} \tag{A.2}$$

$$ATN2_g = \arctan \frac{|d_f| q_g}{\sqrt{p_g u_g - q_g^2}\,\sqrt{w_g}} \tag{A.3}$$

repeatedly used in the sequel. For brevity we shall also set $P_u(\lambda_g) = p_g\lambda_g^2 + 2q_g\lambda_g + u_g$, $P_w(\lambda_g) = P_u(\lambda_g) + d_f^2$.

Denoting by N_{E_f} the number of edges of the face F_f the integrals κ_{F_f} and $\boldsymbol{\kappa}_{F_f}$ have the following expression [52]

$$\begin{aligned}
\kappa_{F_f} &= \int_{F_f} \frac{dA_f}{(\boldsymbol{\rho}_f \cdot \boldsymbol{\rho}_f + d_f^2)^{3/2}} = \frac{\alpha_f}{|d_f|} - \\
&\quad - \sum_{g=1}^{N_{E_f}} \left[\left(\boldsymbol{\rho}_f \cdot \boldsymbol{\nu}_g\right) \int_0^{l_g} \frac{ds_g}{(\boldsymbol{\rho}_f \cdot \boldsymbol{\rho}_f)(\boldsymbol{\rho}_f \cdot \boldsymbol{\rho}_f + d_f^2)^{1/2}} \right] = \\
&= \frac{\alpha_f}{|d_f|} - \sum_{g=1}^{N_{E_f}} \left(\boldsymbol{\rho}_g \cdot \boldsymbol{\rho}_{g+1}^{\perp}\right) \int_0^1 \frac{\lambda_g d\lambda_g}{P_u(\lambda_g)\left[P_w(\lambda_g)\right]^{1/2}} = \\
&= \frac{\alpha_f}{|d_f|} - \sum_{g=1}^{N_{E_f}} \left[\frac{\boldsymbol{\rho}_g \cdot \boldsymbol{\rho}_{g+1}^{\perp}}{|d_f| \sqrt{p_g u_g - q_g^2}} (ATN1_g - ATN2_g) \right]
\end{aligned} \tag{A.4}$$

and

$$\begin{aligned}
\boldsymbol{\kappa}_{F_f} &= \int_{F_f} \frac{\boldsymbol{\rho}_f dA_f}{(\boldsymbol{\rho}_f \cdot \boldsymbol{\rho}_f + d_f^2)^{3/2}} = -\sum_{g=1}^{N_{E_f}} \left(\boldsymbol{\nu}_g \int_0^{l_g} \frac{ds_g}{(\boldsymbol{\rho}_f \cdot \boldsymbol{\rho}_f + d_f^2)^{1/2}} \right) = \\
&= -\sum_{g=1}^{N_{E_f}} \Delta\boldsymbol{\rho}_g^{\perp} \int_0^1 \frac{d\lambda_g}{\left[P_w(\lambda_g)\right]^{1/2}} = -\sum_{g=1}^{N_{E_f}} \hat{I}_g \, \Delta\boldsymbol{\rho}_g^{\perp}
\end{aligned} \tag{A.5}$$

where ν_g is defined in (53) and

$$\begin{aligned}
\hat{I}_g &= \int_0^1 \frac{d\lambda_g}{\left[p_g\lambda_g^2 + 2q_g\lambda_g + w_g\right]^{1/2}} = \\
&= \ln \frac{p_g + q_g + \sqrt{p_g}\,\sqrt{p_g + 2q_g + w_g}}{q_g + \sqrt{p_g w_g}}
\end{aligned} \tag{A.6}$$

The additional integrals referred to in the body of the paper are detailed in the sequel together with their analytical evaluation.

$$\begin{aligned}
I_{0g} &= \int_0^1 \frac{dx}{(p_g x^2 + 2q_g x + w_g)^{3/2}} = \\
&= -\left\{ \frac{p_g x + q_g}{(q_g^2 - p_g w_g)\sqrt{p_g x^2 + 2q_g x + w_g}} \right\}_0^1 = \\
&= \frac{1}{(p_g w_g - q_g^2)} \left(\frac{p_g + q_g}{\sqrt{p_g^2 + 2q_g + w_g}} - \frac{q_g}{\sqrt{w_g}} \right)
\end{aligned} \tag{A.7}$$

$$\begin{aligned}
I_{1g} &= \int_0^1 \frac{x\,dx}{(p_g x^2 + 2q_g x + w_g)^{3/2}} = \\
&= -\left\{ \frac{q_g x + w_g}{(q_g^2 - p_g w_g)\sqrt{p_g x^2 + 2q_g x + w_g}} \right\}_0^1
\end{aligned} \tag{A.8}$$

and the final expression of I_{1g} is

$$\begin{aligned}
I_{1g} &= \frac{q_g + w_g}{(p_g w_g - q_g^2)\sqrt{p_g + 2q_g + w_g}} - \\
&\quad - \frac{w_g}{(p_g w_g - q_g^2)\sqrt{w_g}}
\end{aligned} \tag{A.9}$$

$$\begin{aligned}
I_{2g} &= \int_0^1 \frac{x^2\,dx}{(p_g x^2 + 2q_g x + w_g)^{3/2}} = \\
&= \frac{1}{p_g^{3/2}} \left\{ \frac{\sqrt{p_g}}{(p_g w_g - q_g^2)} \frac{q_g w_g + 2q_g^2 x - p_g w_g x}{\sqrt{p_g x^2 + 2q_g x + w_g}} + \right. \\
&\qquad \left. + \log\left[p_g x + q_g + \sqrt{p_g}\sqrt{p_g x^2 + 2q_g x + w_g} \right] \right\}_0^1 = \\
&= \frac{1}{p_g^{3/2}} \left\{ \frac{\sqrt{p_g}}{(p_g w_g - q_g^2)} \left[\frac{q_g w_g + 2q_g^2 - p_g w_g}{\sqrt{p_g + 2q_g + w_g}} - q_g\sqrt{w_g} \right] + \right. \\
&\qquad \left. + \log\left(\frac{p_g + q_g + \sqrt{p_g}\sqrt{p_g + 2q_g + w_g}}{q_g + \sqrt{p_g w_g}} \right) \right\}
\end{aligned} \tag{A.10}$$

Differently from the previous integrals, the following ones require some preliminary algebraic manipulation.

Actually, to compute

$$I_{3g} = \int_0^1 \frac{dx}{(p_g x^2 + 2q_g x + u_g)(p_g x^2 + 2q_g x + w_g)^{1/2}}$$

we set $t = x + q_g/p_g$ so as to get the simpler expression

$$I_{3g} = \frac{1}{p_g^{3/2}} \int_{q_g/p_g}^{1+q_g/p_g} \frac{dt}{(t^2 + A)\sqrt{t^2 + B}}$$

where

$$\begin{aligned}
A &= \frac{u_g}{p_g} - \frac{q_g^2}{p_g} = \frac{p_g u_g - q_g^2}{p_g^2}, \\
B &= \frac{w_g}{p_g} - \frac{q_g^2}{p_g} = \frac{p_g w_g - q_g^2}{p_g^2}
\end{aligned} \tag{A.11}$$

We thus have

$$I_{3g} = \frac{1}{p_g^{3/2}} \frac{1}{\sqrt{A}\sqrt{B-A}} \arctan\left\{ \frac{t\sqrt{B-A}}{\sqrt{A}\sqrt{B+t^2}} \right\}_{\frac{q_g}{p_g}}^{1+\frac{q_g}{p_g}} =$$
$$= \frac{1}{\sqrt{w_g-u_g}\sqrt{p_g u_g - q_g^2}} \Bigg\{$$
$$+ \arctan \frac{(p_g+q_g)\sqrt{w_g-u_g}}{\sqrt{p_g u_g - q_g^2}\sqrt{p_g+2q_g+w_g}} -$$
$$- \arctan \frac{q_g\sqrt{w_g-u_g}}{\sqrt{p_g u_g - q_g^2}\sqrt{w_g}} \Bigg\} =$$
$$= \frac{1}{|d_f|} \frac{1}{\sqrt{p_g u_g - q_g^2}} \left[ATN1_g - ATN2_g \right] \tag{A.12}$$

since $\sqrt{w_g-u_g} = |d_f|$

Analogously to the integral I_{3g} we transform the integral

$$I_{4g} = \int_0^1 \frac{dx}{(p_g x^2 + 2q_g x + u_g)(p_g x^2 + 2q_g x + w_g)^{3/2}} \tag{A.13}$$

by setting $t = x + q_g/p_g$ to get

$$I_{4g} = \frac{1}{p_g^{5/2}} \int_{q_g/p_g}^{1+q_g/p_g} \frac{dt}{(t^2+A)(t^2+B)^{3/2}} \tag{A.14}$$

In this case one has

$$I_{4g} = \frac{1}{p_g^{5/2}} \Bigg\{ \frac{t}{(A-B)B\sqrt{B+t^2}} +$$
$$+ \frac{1}{\sqrt{A}(B-A)^{3/2}} \arctan\left(\frac{t\sqrt{B-A}}{\sqrt{A}\sqrt{B+t^2}} \right) \Bigg\}_{\frac{q_g}{p_g}}^{1+\frac{q_g}{p_g}} =$$
$$+ \frac{1}{d_f^2(p_g w_g - q_g^2)} \left[\frac{p_g+q_g}{\sqrt{p_g+2q_g+w_g}} - \frac{q_g}{\sqrt{w_g}} \right] +$$
$$+ \arctan \frac{|d_f|\sqrt{p_g}(p_g+q_g)}{\sqrt{p_g u_g - q_g^2}\sqrt{p_g+2q_g+w_g}} -$$
$$- \arctan \frac{|d_f|\sqrt{p_g}q_g}{\sqrt{p_g u_g - q_g^2}\sqrt{w_g}} \tag{A.15}$$

Appendix B. Supplementary material

Supplementary data associated with this article can be found in the online version at “to be specified from the publisher”